Two-way feedback mechanism between unfavorable meteorological conditions and cumulative aerosol pollution exists in various haze regions of China

Junting Zhong[1,2], Xiaoye Zhang[1,3*], Yaqiang Wang[1], Jizhi Wang[1], Xiaojing Shen[1], Hongsheng Zhang[4], Tijian Wang[5], Zhouqing Xie[2,6,7], Cheng Liu[2,6,7], Hengde Zhang[8], Tianliang Zhao[9], Junying Sun[1], Shaojia Fan[10], Zhiqiu Gao[9], Yubin Li[9], Linlin Wang[11]

[1]Chinese Academy of Meteorological Sciences, China Meteorological Administration, Beijing, 100081, China.

[2]University of Chinese Academy of Sciences, Beijing 100049, China

[3]Center for Excellence in Regional Atmospheric Environment, IUE, Chinese Academy of Sciences, Xiamen, 361021, China.

[4]Laboratory for Climate and Ocean-Atmosphere Studies, Department of Atmospheric and Oceanic Sciences, School of Physics, Peking University, Beijing, 100081, China

[5]School of Atmospheric Sciences, Nanjing University, Nanjing, 210023, China

[6]Key Lab of Environmental Optics and Technology, Anhui Institute of Optics and Fine Mechanics, Chinese Academy of Sciences, Hefei, 230031, China

[7]School of Earth and Space Sciences, University of Science and Technology of China, Hefei, 230026, China

[8]National Meteorological Center, China Meteorological Administration, Beijing, 100081, China

[9]Nanjing University of Information Science & Technology, Nanjing, 210044, China

[10]Sun Yat-sen University, Guangzhou, 510275, China

[11]State Key Laboratory of Atmospheric Boundary Layer Physics and Atmospheric Chemistry, Institute of Atmospheric Physics, Chinese Academy of Sciences, Beijing 100029, China

Correspondence to: Xiaoye Zhang (xiaoye@cma.gov.cn)

Abstract. Accompanied by unfavorable meteorological conditions with stable stratification in various haze regions of China, persistent heavy aerosol pollution episodes lasting more than 3 consecutive days (HPEs) frequently occur, particularly in winter. In the North China Plain (NCP), explosive growth in fine particulate matter smaller than 2.5 μm in diameter ($PM_{2.5}$), which occurs in some HPEs, is dominated by a two-way feedback mechanism between further worsened unfavorable meteorological conditions and cumulative aerosol pollution. However, whether such a two-way feedback mechanism exists in other key haze regions is uncertain; these regions include the Guanzhong Plain (GZP), the Yangtze River Delta (YRD) region, the Two Lakes Basin (TLB), the Pearl River Delta (PRD) region, the Sichuan Basin (SB),

and the Northeast China Plain (NeCP). In this study, using surface $PM_{2.5}$ and radiation observations, radiosonde observations, and reanalysis data, we observed the existence of a two-way feedback mechanism in the above six regions. In the SB, this two-way feedback mechanism is weak due to the suppression of cloudy mid-upper layers. In the more polluted NCP, the GZP, and the NeCP, the feedback is more striking than that in the YRD, the TLB, and the PRD. In these regions, the feedback of worsened meteorological conditions on $PM_{2.5}$ explains 60~70% of the increase in $PM_{2.5}$ during the cumulative stages (CSs). For each region, the low-level cooling bias becomes increasingly substantial with aggravating aerosol pollution and a closer distance to the ground surface. With $PM_{2.5}$ mass concentrations greater than 400 μg m^{-3}, the near-ground bias exceeded -4 ºC in Beijing and reached up to approximately -4 ºC in Xi'an; this result was caused by accumulated aerosol mass to some extent. In addition to the increase in $PM_{2.5}$ caused by the two-way feedback, these regions also suffer from the regional transport of pollutants, including inter-regional transport in the GZP, trans-regional transport from the NCP to the YRD and the TLB, and southwesterly transport in the NeCP.

1 Introduction:

In China, 94% of the total population is distributed in eastern China (Yang et al., 2016), in which aerosol pollution has drawn wide attention. In the basins and plains in eastern China, aerosol pollution episodes frequently occur in winter, and these episodes cause economic loss and have adverse effects on human health (Bai et al., 2007;Matus et al., 2012;Chen et al., 2013). For example, in January 2013, persistent heavy aerosol episodes affected 600 million people throughout 1.4 million square kilometers (http://www.infzm.com/content/95493), which led to hundreds of flight cancellations and an increase in the number of reported respiratory disease cases (Ji et al., 2014). During the wintertime (i.e., Jan., Feb., and Dec.) from 2013 to 2017, more than 28 persistent heavy aerosol pollution episodes that lasted for more than 3 consecutive days (HPEs) occurred in Beijing; the peak value of particulate matter smaller than 2.5 μm in diameter (PM2.5) ranged from ~200 μg m^{-3} to ~ 800 μg m^{-3}, with a mean duration longer than 5 days (Zhong et al., 2018a;Zhong et al., 2019). The main cause of frequent pollution episodes is the massive emissions of air pollutants produced by intense living and industrial activities in the basins and plains (Zhang et al., 2009a;Zhang et al., 2012a;Zhang et al., 2013). In addition to pollutant emissions, the relatively closed terrains of basins and plains limit the diffusion of aerosols and their precursors to

the surrounding areas (Su et al., 2004;Zhu et al., 2018). Under stable meteorological conditions, aerosol

pollution forms and further accumulates (Zhang et al., 2013;Zhong et al., 2017).

In winter, unfavorable meteorological conditions lead to aerosol pollution formation, and after

accumulating to some extent, aerosols will change the atmospheric structure by interacting with solar

radiation (Boucher et al., 2013b;Zhong et al., 2018b). The details of the two-way feedback mechanism

between unfavorable meteorological conditions and cumulative aerosols in Beijing are as follows: 1)

When upper zonal large-scale circulations unfavorable for pollution dispersion occur, the boundary layer

(BL) height reduces from ~ 1500 m in clean stages to 700-800 m; under the BL, the winds shift from

northerly to southerly, which transport pollutants from the south of Beijing (transport stages (TSs) in Fig.

1). Above unfavorable meteorological conditions cause aerosol pollution formation. 2). When the vertical

aerosols are accumulated to a certain degree, the dominant scattering aerosols will substantially back-

scatter solar radiation, causing a reduction in the amount of solar radiation that reaches the surface, which

causes a near-ground cooling effect through atmospheric circulation and vertical mixing (i.e., the

cumulative sum of hourly surface vertical and global radiant exposure reduced by 89% and 56%,

respectively, from clean stages to cumulative stages (CSs) (Fig.1)) (Zhong et al., 2017;Zhong et al.,

2018b). With less solar radiation, near-ground temperature subsequently decreases. 3).Under slight or

calm winds, the temperature reduction induces or reinforces an inversion that further weakens turbulence

diffusion and results in a lower BL height, which further worsens aerosol pollution (during CSs in Fig.1).

5). This condition also decreases the near-ground saturation vapor pressure and suppresses water vapor

diffusion to increase the relative humidity (RH), which will further enhances aerosol hygroscopic growth

and accelerates liquid-phase and heterogeneous reactions to worsen aerosol pollution (Pilinis et al.,

1989;Ervens et al., 2011;Kuang et al., 2016;Zhong et al., 2018b;Zhong et al., 2018a). This feedback

effect of further worsened meteorological conditions aggravates $PM_{2.5}$ pollution (during CSs in Fig.1)

(Zhong et al., 2017).
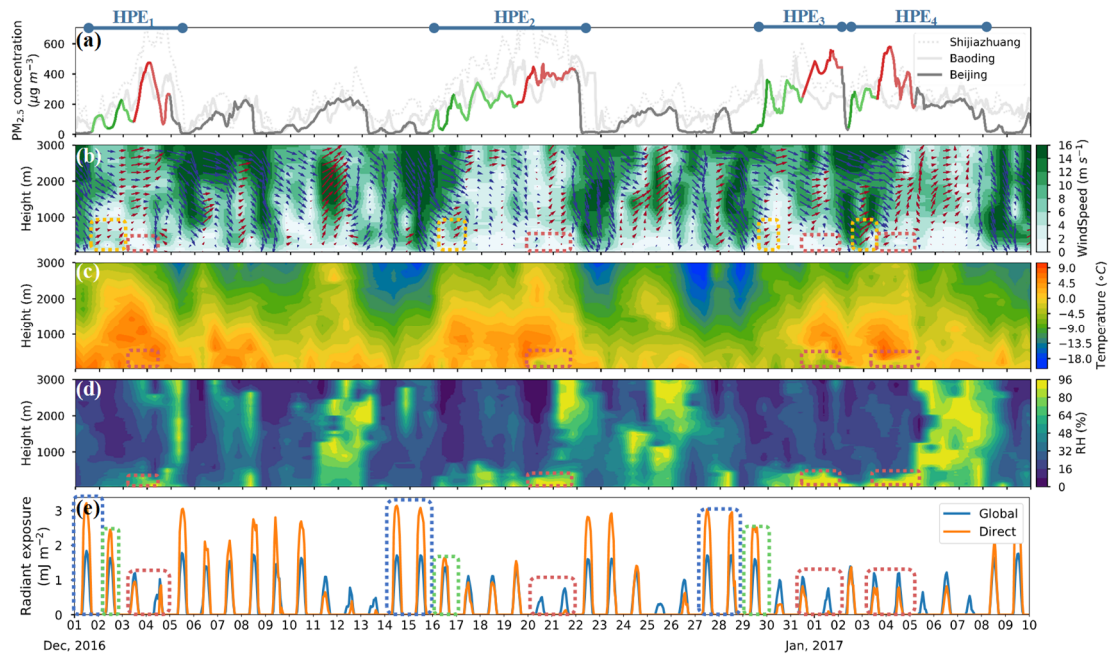
Figure 1: Temporal variations in PM$_{2.5}$, surface radiation, and vertical distributions of meteorological factors from December 1, 2016, to January 10, 2017. (a) PM$_{2.5}$ mass concentration (gray or colored line: Beijing; light gray line: Baoding; gray dot: Shijiazhuang); (b) winds (vectors) and wind velocity (shadings; units: m s^{-1}); (c) temperature (shadings; units: ℃); (d) RH (shadings; units: %); and (e) direct radiant exposure (of the vertical surface to the direction of solar radiation) and global radiant exposure. (Blue line: HPEs; green line and orange box: TSs; red line and white or red box: CSs; blue box: clean periods) *(Adapted from Zhong et al, 2018b)*

The two-way feedback mechanism between unfavorable meteorological conditions and cumulative aerosol pollution also appeared in other cities in the North China Plain, including Tangshan, Xingtai, Zhengzhou and Nanyang (Liu et al, 2018, under review). Whether the two-way feedback mechanism exists in other basins and plains in eastern China, which have weaker aerosol pollution than that in the North China Plain, is unclear. If such feedback exists, its magnitude requires further investigation. Currently, to the best of our knowledge, studies on the existence, magnitude, and comparison of the two-way feedback in these basins and plains are insufficient. Overall, we lack a comprehensive understanding of the feedback mechanism in China. Therefore, here we used surface PM$_{2.5}$ mass concentrations, radiosonde observations of meteorological factors, meteorological index parameter-linking aerosol pollution and meteorological factors (PLAM), and ERA-interim reanalysis data from the European Center for Medium Weather Forecasting (ECMWF) to investigate the two-way feedback mechanism in the key regions of populous eastern China (Yang et al., 2016), including the Guanzhong Plain, the Yangtze River Delta, the Two Lakes Basin, the Pearl River Delta, the Sichuan Basin, and the Northeast China Plain, which are densely populated and economically developed regions that include massive

industrial pollution sources, agricultural pollution sources, motor vehicle pollution sources and domestic pollution sources. In the above regions, heavy aerosol episodes often occur in the regional central cities with denser populations and stronger pollutant emissions, including Xi'an, Nanjing, Shanghai, Wuhan, Guangzhou, Chengdu, and Shenyang. In the above cities, the impact of aerosol pollution episodes on the economy, society, and health is far-reaching. Therefore, we focus on the feedback mechanism in the above cities to represent the overall conditions in the five major haze regions of China, namely, II) the North China Plain (also called Hua Bei Plain) in N. China, plus the Guanzhong Plain; III) E. China with the main body in the Yangtze River Delta area; V) S. China with the most areas of Guangdong and the Pearl River Delta area; IV) The Sichuan Basin in S. W. China, and I) Northeast China Plain (Zhang et al., 2012b) (Fig. 1).

2 Materials and methods:

2.1 PM$_{2.5}$ observations:

Since January 2013, the Ministry of Environmental Protection has been monitoring the PM$_{2.5}$ mass concentrations in real time at over 1000 environmental monitoring stations established in different regions of China. In this study, we used the hourly PM$_{2.5}$ mass concentrations provided by the Ministry of Environmental Protection from December 1, 2016 to January 10, 2017 and the respective averaged PM$_{2.5}$ mass concentrations of all the urban stations in Xi'an, Yuncheng, Shenyang, Chengdu, Wuhan, Nanjing, Shanghai, Jinan, Guangzhou and Qingyuan. The in situ monitoring data of the hourly concentrations of PM$_{2.5}$, PM$_{10}$, CO, NO$_2$, SO$_2$, and O$_3$ are acquired from the national air quality real-time publishing platform (http://106.37.208.233:20035).

We also used an unmanned aerial vehicle to observe PM2.5 mass concentration at different heights within 1 km every three hours in Nanjing from December 3 to 4, 2017. The data were obtained with the UAV platform-CEEWA X8 (Nanjing CEEWA Intelligent Technology Co., Ltd., Nanjing, China), a six-rotor industrial UAV carrying highly reliable, triple-redundant FC-IU3 flight control system (Zhou et al., 2018). On the platform, a multiparameter atmospheric environment detector was equipped, which was developed by Shenzhen TENGWEI Measurement and Control Technology Co., Ltd., Shenzhen, China (Zhou et al., 2018). The experiment was performed on the Xianlin campus of Nanjing University. This campus is located in the eastern suburb of Nanjing and surrounded by farmland, residential areas, and

small patches of forest and chemical plants. The experiment site was located on a playground without tall structures surrounded.

2.2 Meteorological radiosonde observations:

In China, 120 stations have been observing vertical meteorological factors using L-band sounding radars. Their accurately positioned radar systems collect reliable meteorological data each second; thus, these data have high spatial and temporal resolutions (Tao, 2006). In this study, we used the L-band sounding radar data from the meteorological stations in Xi'an, Shenyang, Chengdu, Wuhan, Nanjing, Shanghai, and Qingyuan; these stations observed several meteorological factors, including wind, temperature and RH, twice each day at 0800 (BJT) and 2000 (BJT) from December 1, 2016 to January 10, 2017. The meteorological factors were analyzed in detail below the height of 3 km. The heights from the surface to 1 km, from 1 km to 2 km, and from 2 km to 3 km are termed the low-level, mid-level, and upper-level heights, respectively. In addition, due to the lack of meteorological radiosonde observations in Guangzhou, we supplemented related observations in its adjacent city, Qingyuan.

2.3 Surface meteorological data:

Since 2001, national weather stations have been conducting automatic hourly observations. Some of the stations began to record observations every 5 and 10 minutes starting in 2011. This study used the hourly meteorological observation data, including temperature, pressure, RH, wind, and visibility at the National Automatic Weather Stations (AWS) provided by the National Meteorological Information Center of China Meteorological Administration (NMICMA). The time range of the selected data is from December 1, 2016, to January 10, 2017.

We also used an hourly radiant exposure data set of national meteorological radiation factors (V2.0) provided by the NMICMA. This dataset contains 104 radiation stations, including primary stations with global, direct, scattered, reflected, and net radiation, secondary stations with global and net radiation, and tertiary stations with only global radiation. These radiation stations recorded hourly basic radiant exposure data and the corresponding station information (i.e., latitude, longitude, and altitude) starting in 1993. In this study, we used the global, direct and net radiant exposure from December 1, 2016, to January 10, 2017.

2.4 PLAM data

Based on the definition and calculation formula of PLAM (a parameter that links aerosol pollution and meteorological factors) (Zhang et al., 2009b;Wang et al., 2012;Wang et al., 2013;Zhang et al., 2015), we obtained the PLAMs in Xi'an, Nanjing, Wuhan, Qingyuan, Chengdu, and Shenyang using surface meteorological factors. PLAM includes two major separate factors: (1) the initial meteorological conditions α(m) associated with the atmospheric condensation processes and (2) an effective dynamic parameter associated with the initial contribution of air pollution β(c'):

$$PLAM = α(m) × β'(c). \tag{1}$$

This calculation mainly indicates regional atmospheric stability and air condensation ability. The details of the calculation have been presented in previous studies (Wang et al., 2012;Wang et al., 2013).

2.5 ECMWF ERA-Interim data

ERA-Interim is ECMWF's latest global atmospheric reanalysis, which extends back to 1979 and continuously updates in real time (Dee et al., 2011). It is produced with a 4-dimensional variational data assimilation scheme and advances forward in time using 12-hour analysis cycles (Thépaut et al., 1996;Dee et al., 2011). Before assimilation, all data are subject to gross, redundancy and background quality controls, which resulted in a large drop between the total number of available data and the number of data used in the assimilation. The mean daily usage rate of radiosondes is no more than 50% over the entire period (Poli et al., 2010). In addition, although the effect of aerosols on radiative transfer in the atmosphere is modeled based on prescribed climatological aerosol distributions (Dee et al., 2011), it has not considered the two-way feedback mechanism between the cumulated aerosol pollution and the worsened meteorological conditions (Simmons, 2006). Therefore, the magnitude of the feedback mechanism could be statistically reflected by the gaps between the ERA-interim reanalysis and the meteorological radiosonde observations. The disparities have been used to present the observational evidence of aerosol-PBL interactions in Beijing (Ding et al., 2016;Huang et al., 2018).

In this study, we used ERA-Interim data with a horizontal resolution of 0.125° × 0.125°. Its mandatory pressure levels include 1000, 975, 950, 925, 900, 875, 850, 825, 800, 775, 750, and 700 hPa. According to these pressure layers, we interpolated the radiosonde observations and calculated the vertical temperature differences between the ERA-interim reanalysis and the interpolated sounding data at 20:00 (BJT).

3 Results and Discussions:

Based on the consistent variation trends in visibility, China is classified into nine typical regions (Zhang et al., 2012b). Five of these regions have experienced striking declines in visibility in recent decades, including (1) the North China Plain and the Guanzhong Plain in North China; (2) the Yangtze River Delta region and the Two Lakes Basin along the middle and lower reaches of the Yangtze River; (3) the Pearl River Delta region in South China; (4) the Sichuan Basin in Southwest China; (5) and the Northeast China Plain (Fig. 2). The areas with declined visibility coincide with the basins and plains in eastern China because these basins and plains are densely populated and topographically enclosed; additionally, these areas emit and produce massive air pollutants, including primary aerosols and secondary aerosols from gas-to-particle conversion. These aerosols locally accumulate to continuously reduce visibility. By comparing the mean $PM_{2.5}$ mass concentration from December 1, 2016 to that of January 10, 2017 in the five regions that experienced declines in visibility (Fig. 3), we found that the heaviest aerosol pollution occurred in the North China Plain, and it was followed by the Guanzhong Plain. The areas with the next highest aerosol pollution were the Sichuan Basin and the Northeast China Plain. The Two Lakes Basin and the Yangtze River Delta experienced less aerosol pollution. Finally, the Pearl River Delta had the least aerosol pollution.
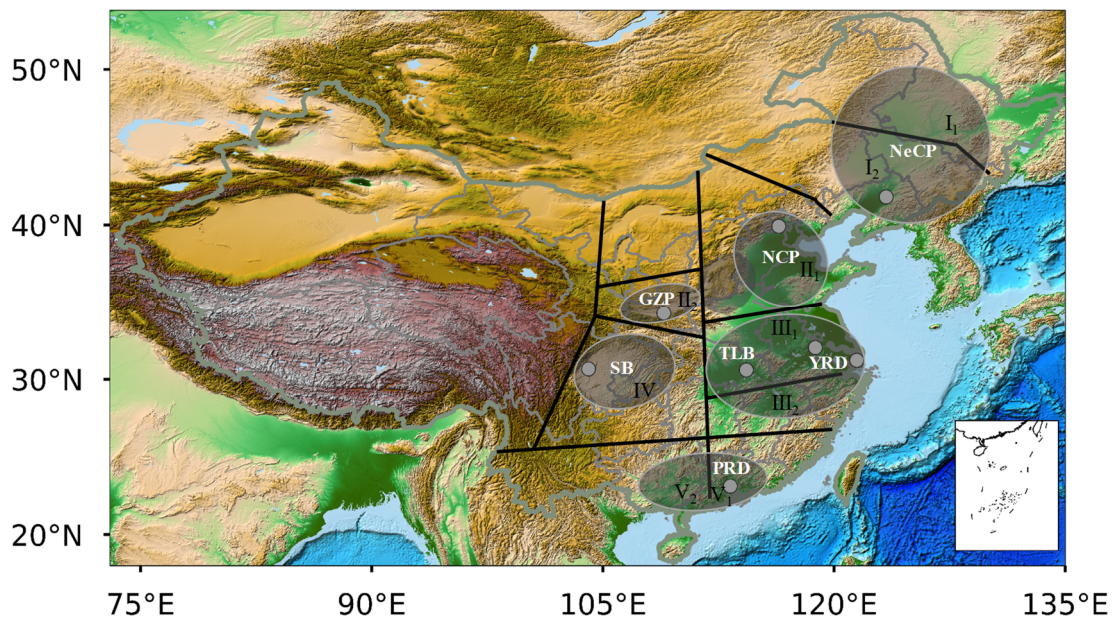
Figure 2: The key haze regions with similar declines in visibility in eastern China. (White dot: locations of radiosonde stations)
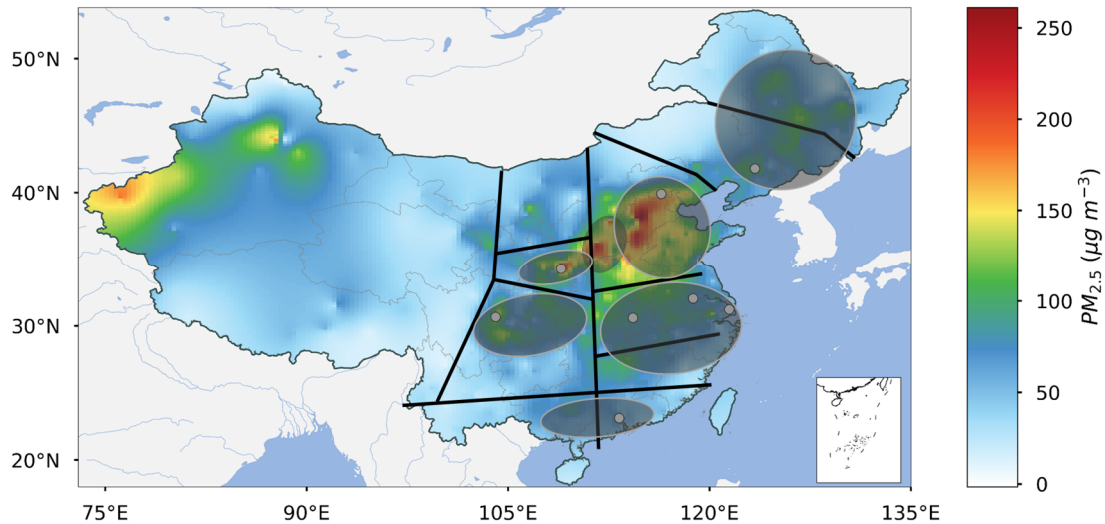
Figure 3: National distribution of mean PM₂.₅ mass concentration from December 1, 2016, to January 10, 2017. (White dot: locations of radiosonde stations)

3.1 Striking two-way feedback in the polluted Guanzhong Plain with inter-regional pollution transport.

To the north of the Loess Plateau and the south of the Qinling Mountains, the Guanzhong Plain has a narrow and closed terrain (Fig. 2), and its climatic and meteorological conditions are distinctive from those of the surrounding areas. Compared with the plateau to the north, the Guanzhong Plain is less affected by northerly cold and clean winds, and these conditions favor the accumulation of pollutants. However, because the Loess Plateau is lower in elevation than the Hengduan Mountains and the Daba Mountains located to the northwest of the Sichuan Basin, the barrier effect of the plateau on the northerly cold air is weaker than that of those mountains (Fig. 4 (b) and Fig. 12 (b)). Because the North China Plain is bordered to the west by the Taihang Mountains and the Lvliang Mountains (Fig. 2), the Guanzhong Plain is rarely affected by pollutant transport from the North China Plain; however, air pollution is highly correlated among the different cities in the Guanzhong Plain. To the west of this plain, Xi'an lies north of the Wei River and the Loess Plateau and south of the Qinling Mountains (Fig. 2). Due to its enclosed topography, Xi'an frequently experiences heavy urban aerosol pollution.
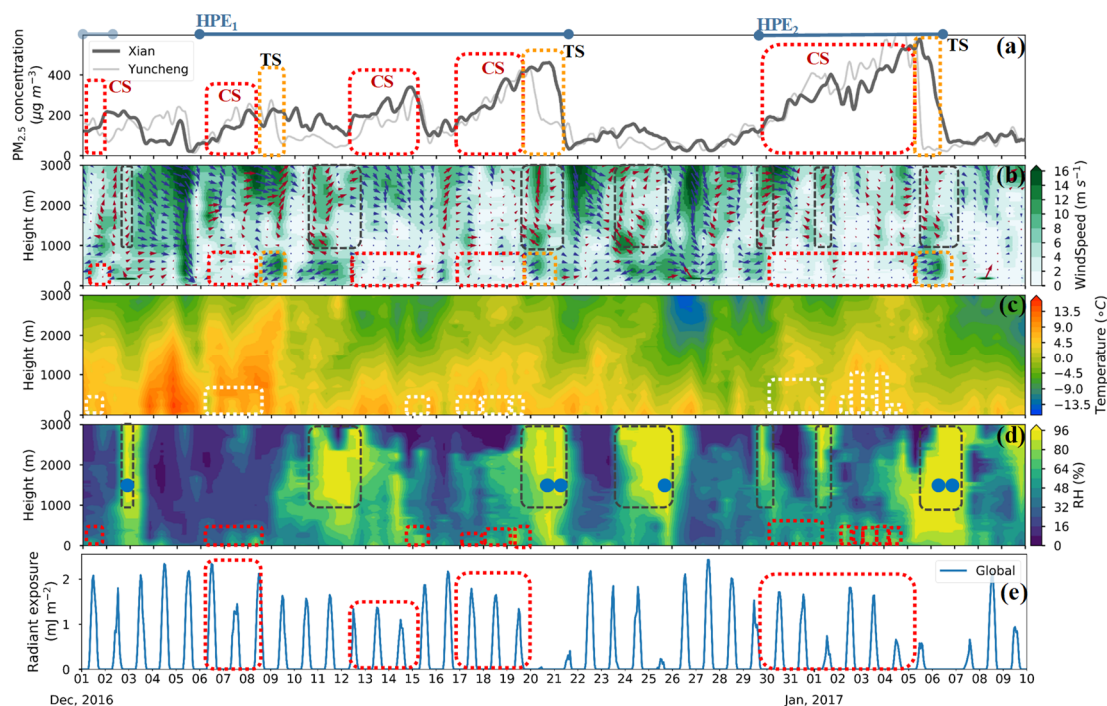
Figure 4: Temporal variations in PM$_{2.5}$, surface radiation, and vertical distributions of meteorological factors from December 1, 2016, to January 10, 2017. (a) PM$_{2.5}$ mass concentration (gray line: Beijing; light gray line: Yuncheng); (b) winds (vectors) and wind velocity (shadings; units: m s^{-1}); (c) temperature (shadings; units: ℃); (d) RH (shadings; units: %); and (e) global radiant exposure. (Blue line: HPEs; light blue line: PEs; white or red box: CSs; and brown box: water vapor transport)

From December 1, 2016, to January 10, 2017, two HPEs appeared in Xi'an and persisted for more than 7 days with peak mass concentrations greater than 400 μg m^{-3} (Fig. 4 (a), dark blue lines). During HPE$_{1-2}$, we observed a striking two-way feedback mechanism between the worsened weather conditions and the cumulated aerosol pollution (Fig. 4, red and white boxes). When the near-ground PM$_{2.5}$ accumulates to a certain extent, the particles scatter more solar radiation back to space, which substantially reduces the surface radiation (Fig. 4 (e), red boxes) and consequently lowers the near-surface temperature (Fig. 4 (c), white boxes). Under slight or calm winds (Fig. 4 (b), red boxes), the temperature reduction induces or reinforces inversions, which further weaken turbulence diffusion to suppress the diffusion of water vapor and pollutants (Zhong et al., 2017;Zhong et al., 2018a); these conditions also decrease the near-ground saturation vapor pressure to increase the RH (Fig. 4 (d), red boxes), which further enhances aerosol hygroscopic growth and accelerates liquid-phase and heterogeneous reactions (Cheng et al., 2016;Fang et al., 2016;Tie et al., 2017). This type of two-way feedback mechanism leads to worsened meteorological conditions and elevated PM$_{2.5}$ mass concentrations.

To quantify the magnitude of the two-way feedback during TSs and CSs in polluted Beijing and

250   Xi'an, we obtained the air temperature difference between the radiosonde observations at 2000 BJT

251   affected by this two-way feedback (whose temperature profiles were more affected by aerosols' blocking

252   in solar radiation transfer compared with observations at 0800 BJT) and the ERA-interim reanalysis data

253   without the feedback. We found that the temperature profile was modified by aerosols during both the

254   TSs and the CSs in Beijing and Xi'an (Fig.5 (a, b)). However, a comparison of aerosol-induced

255   temperature modification in the TSs and the CSs indicates that the lower cooling bias was more striking

256   in the CSs, which also became increasingly substantial with a closer distance to the ground surface. From

257   TSs to CSs, the negative temperature difference at 1000 hPa increased from -0.8 ℃ to -4.3 ℃ and

258   from -1.3 ℃ to -2.7 ℃ in Beijing and Xi'an respectively. Using the near-ground temperature reduction

259   (1000 hPa) as an index to evaluate the magnitude of the two-way feedback from TSs to CSs, we found

260   that during TSs the aerosol-induced cooling bias was 18.6% and 48.7% of the difference during CSs in

261   Beijing and Xi'an respectively. It is expectable because from the TSs to the CSs aerosol pollution

262   worsened with increasing radiative cooling effects. Moreover, though relatively strong winds in the TSs

263   were conducive to pollution transport, they were unfavorable for the formation and maintenance of stable

264   stratification, in which occurred aerosol self-induced pollution deterioration frequently.
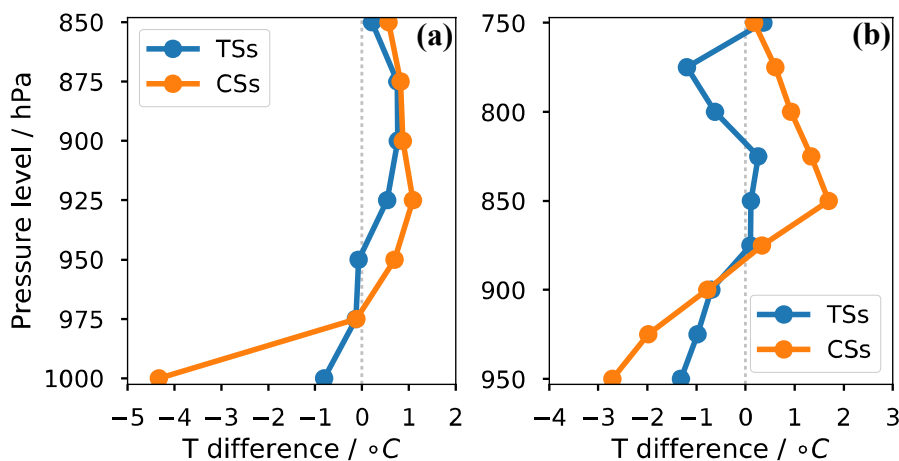
265

266   **Figure 5: Vertical mean temperature difference between sounding observations and ERA-interim reanalysis**

267   **data during TSs and CSs from December 1, 2016, to January 10, 2017.** (a) Beijing; (b) Xi'an

268   During HPE$_{1-2}$, we also observed an increase in the PM$_{2.5}$ mass concentration caused by pollutant

269   transport. The aerosol pollution in Xi'an might be aggravated by the transport of pollutants from the

270   eastern polluted plain area with heavily polluted cities, including Yuncheng and Linfen. To reveal the

271   effects of air pollutant transport from the eastern plain on the aerosol pollution in Xi'an, we compared

272   the variation trends in the PM$_{2.5}$ mass concentrations in Xi'an and Yuncheng under lower northwesterly

winds (Fig. 4 (a, b)). We found that during TSs in Fig. 4 (orange boxes), low-level northwesterly winds would transport pollutants below the BL to maintain or aggravate the aerosol pollution in Xi'an when Yuncheng is heavily polluted; however, when Yuncheng had good air quality, the aerosol pollution in Xi'an was lighter or even eliminated.

In addition to the scavenging effect of clean northwesterly winds on aerosol pollution, pollution elimination mainly depends on lower strong northwesterly winds and mid-upper level southerly winds. Because the Loess Plateau north of Xi'an is sparsely populated with rare air pollutant emissions, lower strong and clean northwesterly winds would blow away aerosol pollutants in Xi'an, causing a subsequent rapid improvement in the air quality (Fig. 4 (a, b)). Since the mid-upper level southerly winds transport water vapor to Xi'an from the area south of Xi'an, the mid-upper (or whole-layer) RH level is considerably enhanced (i.e., greater than 96%) (Fig. 4 (b, d), brown boxes), which causes the $PM_{2.5}$ to enter the fog-cloud phase and possibly produces precipitation that eliminates pollutants through wet removal (Fig. 4 (d), blue dots represent precipitation).

3.2 Affected by trans-regional pollution transport from the North China Plain, the Yangtze River Delta region subsequently experiences the two-way feedback.

Located in the lower reaches of the Yangtze River, the Yangtze River Delta is a triangle-shaped metropolitan region. It covers an area of 211,700 km^{-2} and is home to more than 150 million people as of 2014 (http://www.ndrc.gov.cn/zcfb/zcfbghwb/201606/t20160603_806390.html). The urban build-up in this area has given rise to what may be the largest concentration of adjacent metropolitan areas in the world. The Yangtze River Delta has a marine monsoon subtropical climate with cool and dry winters. Situated in the Yangtze River Delta, Nanjing is the second largest city in the East China region. The south, north, and east sides of the city are surrounded by the Ningzheng Ridges (Fig. 2), while the Yangtze River flows along the west and part of the north sides.
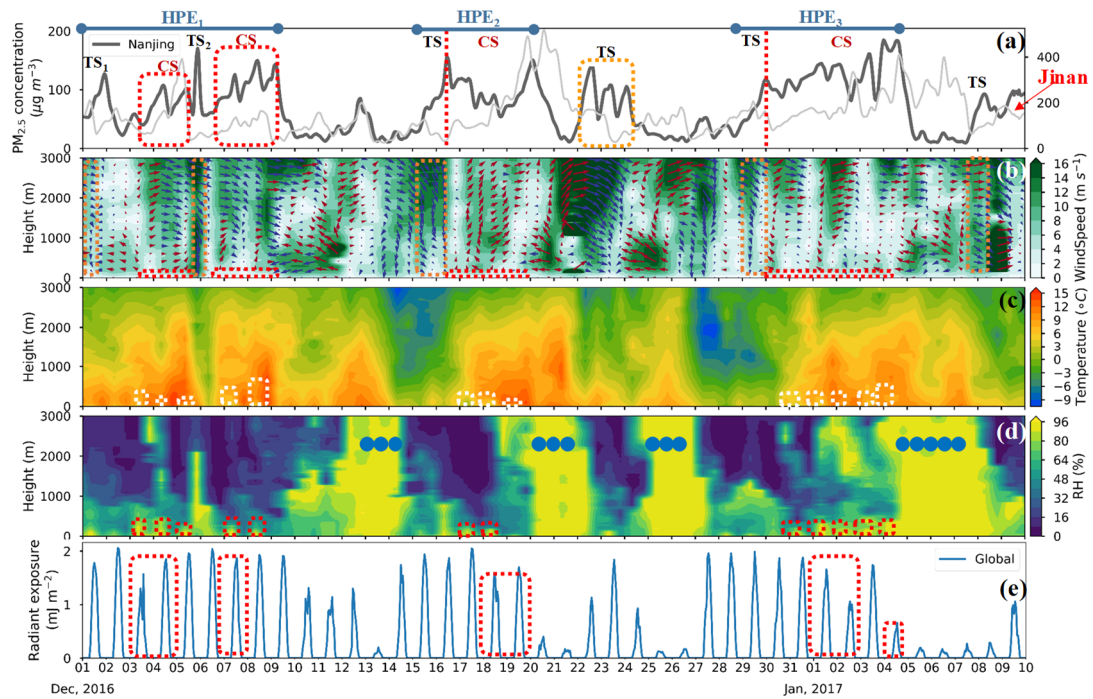
Figure 6: Temporal variations in PM₂.₅, surface radiation, and vertical distributions of meteorological factors from December 1, 2016, to January 10, 2017. (a) PM₂.₅ mass concentration (gray line: Nanjing; light gray line: Jinan); (b) winds (vectors) and wind velocity (shadings; units: m s⁻¹); (c) temperature (shadings; units:°C); (d) RH (shadings; units: %); and (e) global radiant exposure. (Blue line: HPEs; light blue line: PEs; white or red box: CSs; and blue dot: precipitation.)

From December 1, 2016, to January 10, 2017, four aerosol pollution episodes occurred in Nanjing (Fig. 6 (a), blue boxes). One of these episodes lasted for less than 3 days and had light pollution, while the other three episodes persisted for more than 5 days and had peak mass concentrations greater than 150 μg m⁻³; thus, these three episodes are termed HPEs (Fig. 6 (a)). During these three HPEs, although the PM₂.₅ mass concentration was much lower than that in Beijing, the aerosol pollution formation was similar to that in the latter, including earlier TSs and later CSs (Zhong et al., 2017;Zhong et al., 2018a). During the TSs in the HPEs, strong northerly winds transport aerosol pollutants from the polluted North China Plain to the Yangtze River Delta region below and over the BL (i.e., long-distance pollution transport), which induces a striking increase in the PM₂.₅ mass concentration in Nanjing and a reduction in the PM₂.₅ mass concentration in Jinan, a regional center city representative of the pollution conditions in the NCP (Fig. 6 (a, b)). To some extent, based on the PM₂.₅ mass, the two-way feedback mechanism is activated during the CSs, in which we observed surface radiation reductions, near-surface inversions, low-layer RH enhancement, and increased PM₂.₅ mass concentrations under slight winds (Fig. 6). Due to the lighter aerosol pollution in Nanjing, the two-way feedback mechanism is weaker than that in Beijing (Fig. 1, 6 (a)). In addition, the mechanism might be weakened by relatively strong lower winds (compared

317   to those in Beijing) (Fig. 1, 6 (b)), which are unfavorable for the accumulation of aerosols.
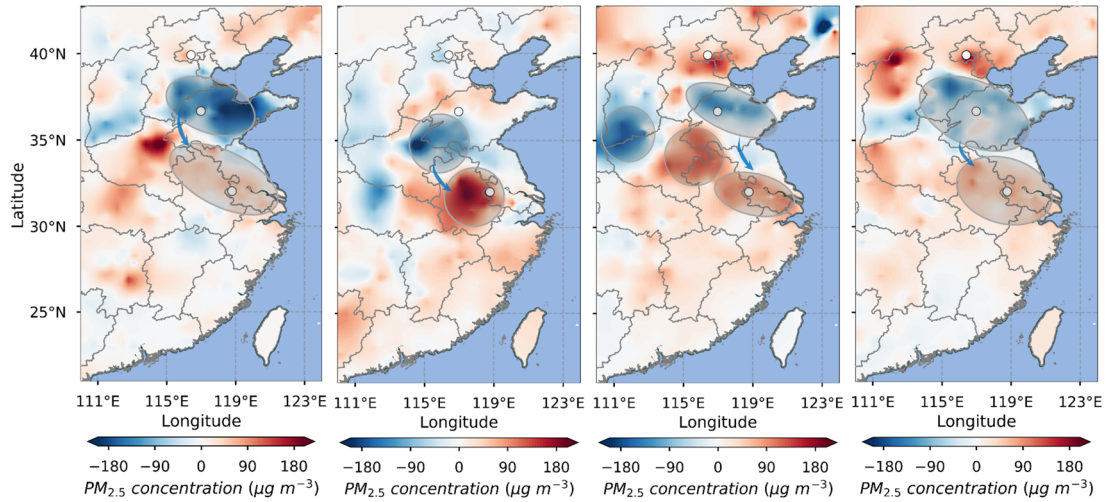
318

319   **Figure 7: The distribution of the concentration differences in PM$_{2.5}$ mass between the start time and the end**
320   **time (the end is subtracted from the start) of the TSs in Figure 4.** (a) TS$_1$ in HPE$_1$; (b) TS$_2$ in HPE$_1$; (c) TS in
321   HPE$_2$; and (d) TS in HPE$_3$.

322   To reveal the regional pollutant transport patterns from the North China Plain to the Yangtze River

323   Delta region, we calculated the concentration difference in the PM$_{2.5}$ mass between the start time and the

324   end time of the TSs in HPE$_{1,2,4}$ (Fig. 7). We found that the southern area of the North China Plain

325   experienced a substantial reduction in its PM$_{2.5}$ mass concentration, while an increase occurred in the

326   middle and lower reaches of the Yangtze River, including the Two Lakes Basin and the Yangtze River

327   Delta region; these results indicate the process of regional pollutant transport from the North China area

328   to the East China area under strong northwesterly winds. In the winter of 2017, we also observed this

329   pollution transport (Fig. 6, orange boxes), As shown in Fig. 8, we observed mid-level pollutants transport

330   at the beginning of the TS, after which near-surface PM$_{2.5}$ reaches the highest concentration with

331   downward mixing. Subsequently, another northerly pollutant transport reached middle layers over

332   Nanjing. Afterward, persistent northerly winds blew pollutants away (Fig. 8, purple boxes). In addition

333   to the blowing effect of persistent northerly winds, eliminating pollution in Nanjing mainly depends on

334   strong southeasterly winds, which transport warm, humid, and clean air from the Yellow Sea and the East

335   China Sea; this air also blows the aerosol pollutants in Nanjing away (Fig. 6 (b, c, d)). In addition,

336   transported water vapor increases the RH (Fig. 6 (b, d)), which causes the PM$_{2.5}$ to enter the fog-cloud

337   phase and possibly produces precipitation that eliminates pollutants through wet removal (Fig. 6 (d), blue

338   dots represent precipitation).
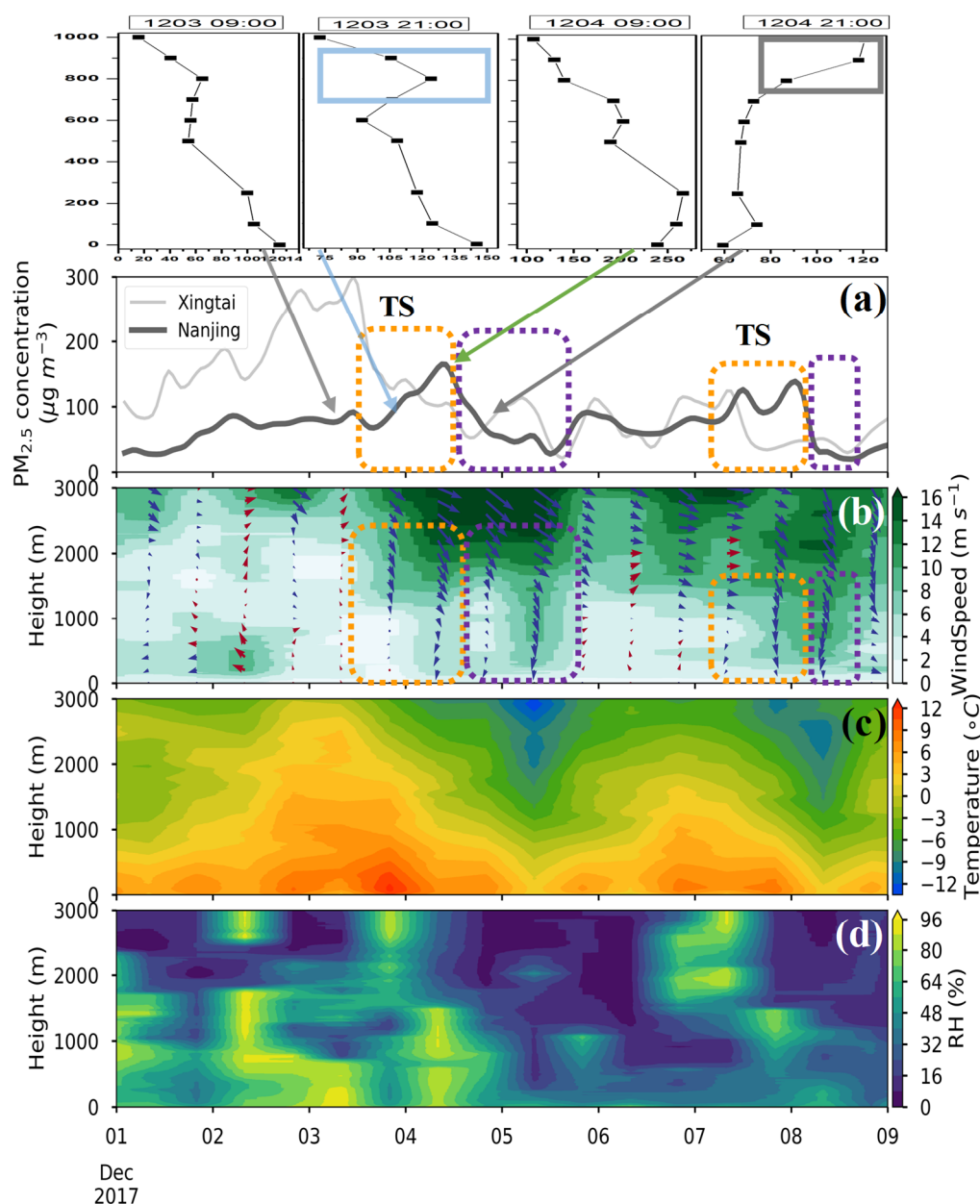
Figure 8: Temporal variations in PM$_{2.5}$ and vertical distributions of meteorological factors from December 1, 2017 to December 9, 2017. (a) PM$_{2.5}$ mass concentration (gray line: Nanjing; light gray line: Xingtai); (b) winds (vectors) and wind velocity (shadings; units: m s^{-1}); (c) temperature (shadings; units: ℃); and (d) RH (shadings; units: %). (Orange box: TSs; purple box: clean periods)

Consistent with the results observed in Nanjing, Shanghai also experienced long-distance pollution transport below and over the BL under northwesterly winds (Fig. 9 (a, b), orange boxes). After PM$_{2.5}$ accumulated to some extent, we observed a two-way feedback mechanism, including reduced radiation, near-surface inversions, RH enhancement in the lower parts of BL, and increase in PM$_{2.5}$ mass concentration under slight or calm winds (Fig. 9 (a, b, c, d, e) red and white boxes); however, the magnitude of the feedback was weaker than that observed in Nanjing (Fig. 6). Because Shanghai is closer

350 to the sea than Nanjing, it is more susceptible to warm, humid southeasterly winds from the sea, which

351 carry more water vapor to Shanghai than to Nanjing (Figs. 6 & 9 (b, d)).
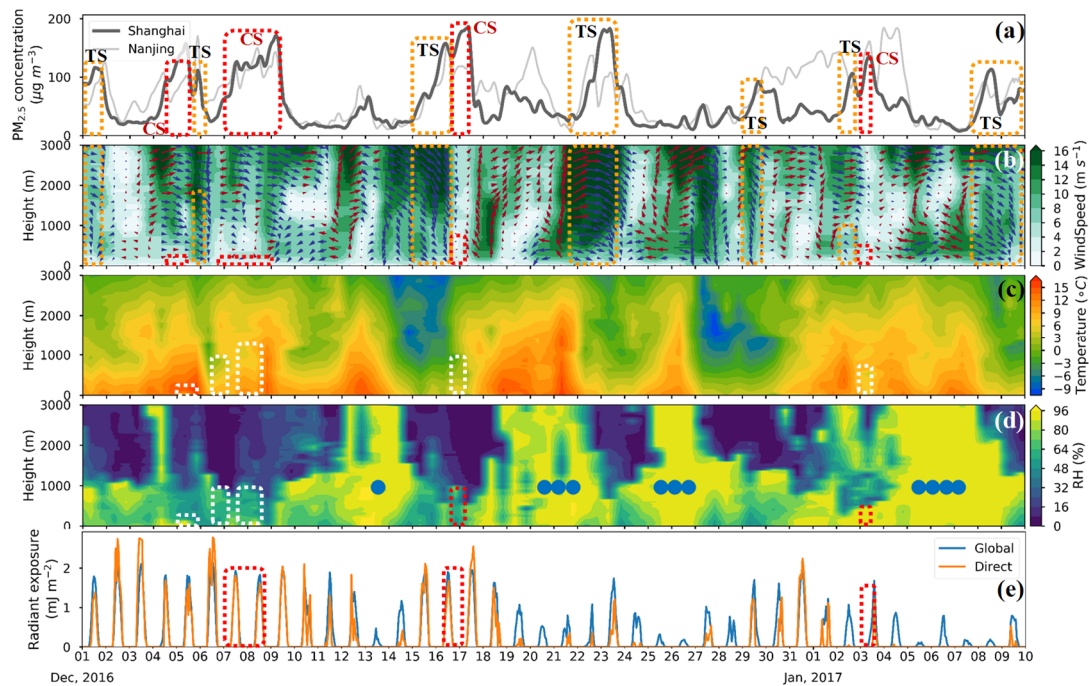
352

353 **Figure 9: Temporal variations in PM$_{2.5}$, surface radiation, and vertical distributions of meteorological**

354 **factors from December 1, 2016, to January 10, 2017.** (a) PM$_{2.5}$ mass concentration (gray line: Shanghai; light

355 gray line: Nanjing); (b) winds (vectors) and wind velocity (shadings; units: m s^{-1}); (c) temperature (shadings;

356 units: °C); (d) RH (shadings; units: %); and (e) direct radiant exposure (of the vertical surface to the direction of

357 solar radiation) and global radiant exposure. (White or red box: CSs; orange box: TSs; and blue dot: precipitation)

358 **3.3   The two-way feedback exists in the Two Lakes Basin, in which aerosol pollution is also**

359 **worsened by the trans-regional pollution transport from the North China Plain.**

360   The Two Lakes Basin is in the middle reaches of the Yangtze River. With the Sichuan Basin

361 bordered to the northwest by the Daba Mountains (Fig. 2), the Two Lakes Basin is rarely affected by

362 pollutant transport from polluted cities in Sichuan Basin. The north side of the Two Lakes Basin is

363 connected to the North China Plain through the Suizhou Corridor and the Nanyang Basin (Fig. 2); thus,

364 the Two Lakes Basin is vulnerable to pollution transport from the North China Plain, which experiences

365 the heaviest aerosol pollution in China (Fig. 3). As a large exorheic basin surrounded by low ridges or

366 mountains, the Two Lakes Basin more frequently exchanges air masses with its surroundings, with wind

367 speeds much higher than those in Sichuan Basin. Situated in the eastern Two Lakes Basin, Wuhan is the

368 most populous city in Central China. The Yangtze and Han rivers wind through this city, which has a

369 southern hilly and middle flat terrain (Fig. 2).
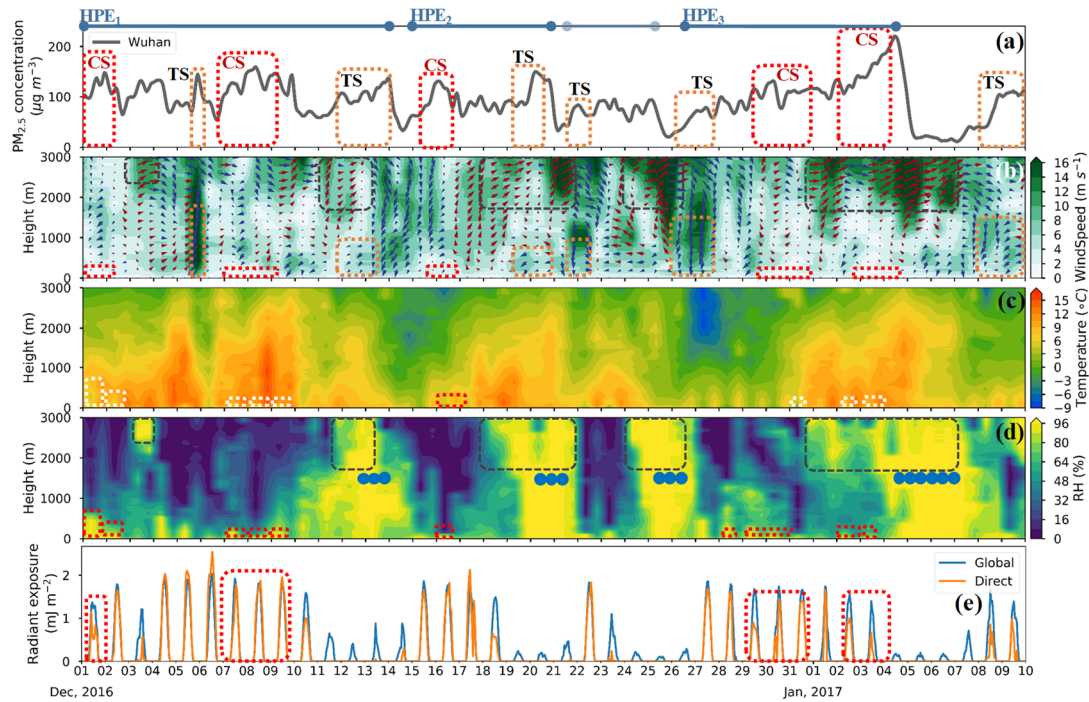
Figure 10: Temporal variations in PM$_{2.5}$, surface radiation, and vertical distributions of meteorological factors from December 1, 2016 to January 10, 2017. (a) PM$_{2.5}$ mass concentration (gray line: Wuhan); (b) winds (vectors) and wind velocity (shadings; units: m s^{-1}); (c) temperature (shadings; units: °C); (d) RH (shadings; units: %); and (e) direct radiant exposure (of the vertical surface to the direction of solar radiation) and global radiant exposure. (Blue line: HPEs; light blue line: PEs; white or red box: CSs; orange box: TSs; brown box: water vapor transport; and blue dot: precipitation.)

From December 1, 2016 to January 10, 2017, four aerosol pollution episodes occurred in Wuhan (Fig. 10 (a), blue boxes). Three of these episodes lasted longer than 5 days and had peak mass concentrations greater than 150 μg m^{-3}, which are termed HPEs (Fig. 10 (a)). During these three HPEs, we observed a two-way feedback mechanism in the red boxes (Fig. 10), including surface radiation reductions, near-surface inversions, low-level RH enhancement, and increases in PM$_{2.5}$ mass concentrations under slight or calm winds (Fig. 10). Similar to the conditions observed in Nanjing, Wuhan experienced lighter aerosol pollution than Beijing (Fig. 1, 10 (a)); thus, the two-way feedback mechanism is weaker than that observed in Beijing.

Figure 7 shows the regional pollutant transport from the North China Plain to the Two Lakes Basin, which also aggravates the PM$_{2.5}$ pollution in Wuhan. As shown in the orange boxes of Fig. 10, the lower northerly winds transport pollutants from the north of Wuhan to below Wuhan and sometimes over the BL, which results in increasing PM$_{2.5}$ mass concentrations. Therefore, favorable northerly winds establish a pollution linkage between the North China Plain and the middle and lower reaches of the Yangtze River (including the Yangtze River Delta and the Two Lakes Basin), which have low and flat

terrains (Fig. 2). However, if the northerly winds are persistent and strong enough, they will blow the aerosol pollutants out of the North China Plain entirely and then transport clean and cold winds to Wuhan; under these conditions, the PM$_{2.5}$ mass concentration first increases and then decreases dramatically. This phenomenon was observed from December 12 to 14, 2016 and is shown in Fig. 10.

In addition to the blowing effect of the strong, persistent northerly winds, clearing the pollution in Wuhan mainly depends on the mid-upper level southerly winds, particularly the southwesterly winds, which transport water vapor to Wuhan from the south, substantially enhancing the RH (over 96%) (Fig. 10 (b, d), brown boxes); these conditions cause the PM$_{2.5}$ to enter the fog-cloud phase and often produce precipitation that eliminates pollutants through wet removal (Fig. 10 (d), blue dots represent precipitation).

3.4   The two-way feedback in the less polluted Pearl River Delta region, which is also humidified by upper southerly winds from the South China Sea and purified by lower clean, cold northeasterly winds.

Located in the southeastern area of Guangdong Province, the Pearl River Delta is one of the most populous and densely urbanized regions in the world. This low-lying area is surrounded by the Pearl River estuary, where the East River, West River, and North River converge to flow into the South China Sea. With the South China Sea to its south, the Pearl River Delta region is often influenced by southerly sea winds; however, with the mountainous area in northern Guangdong to the north (Fig. 2), the Pearl River Delta region is less affected by northerly cold and clean winds. Situated at the heart of the Pearl River Delta region (Fig. 2), Guangzhou is the most populous city of Guangdong Province. However, due to the lack of a meteorological radiosonde station in Guangzhou, we used the sounding observations from Qingyuan, a city with similar PM$_{2.5}$ variation trends (Fig. 9 (a)); Qingyuan is located approximately 60 km to the north of Guangzhou.

From December 1, 2016, to January 10, 2017, the PM$_{2.5}$ mass concentration in Guangzhou and Qingyuan is ~50 μg m^{-3}, which is much lower than that in Xi'an, Nanjing, Wuhan, Chengdu, and Shenyang. During this period, only one HPE occurred, and it lasted for more than 8 days with a peak mass concentration of approximately 150 μg m^{-3} (Fig. 11, blue line). During this episode, we observed surface radiation reductions, near-surface inversions, low-level RH enhancement, and increases in the PM$_{2.5}$ mass concentration under slight or calm winds (Fig. 11, red/white boxes below the blue line),

which suggest that a two-way feedback mechanism exists in the region. Except for this episode, we found

that the PM$_{2.5}$ mass concentration increased during slight or calm winds but was still below the threshold

(Fig. 11, the red boxes before Jan 1, 2017) (Zhong et al., 2019); thus, no inversion or increased RH

occurred because the two-way feedback mechanism was not effectively activated.
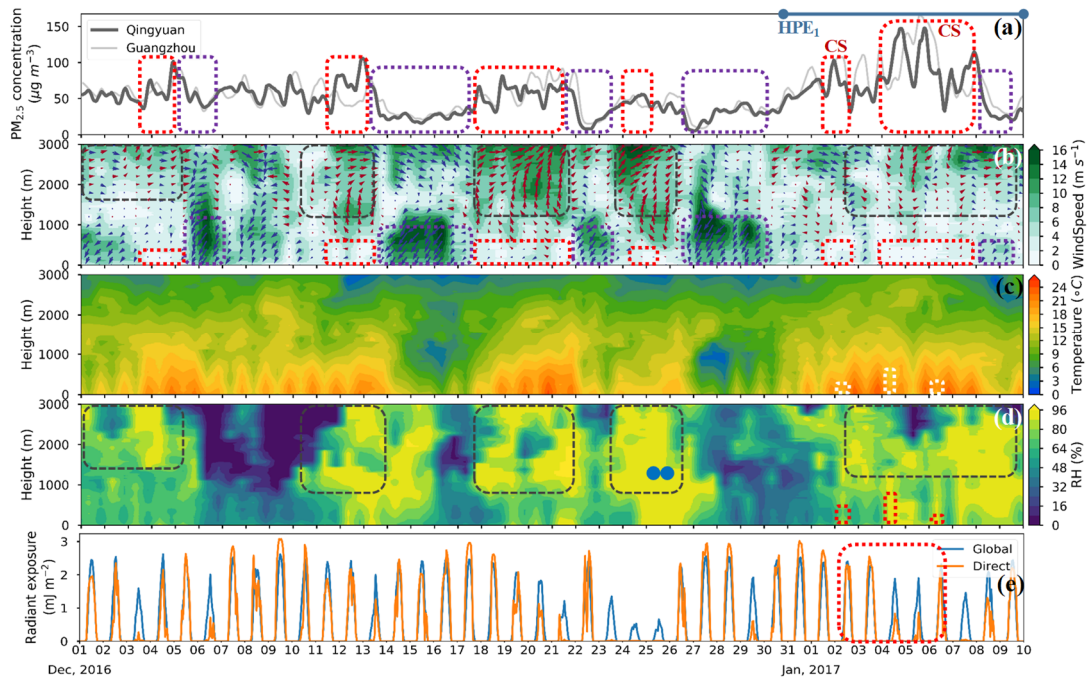
Figure 11: Temporal variations in PM$_{2.5}$, surface radiation, and vertical distributions of meteorological factors from December 1, 2016 to January 10, 2017. (a) PM$_{2.5}$ mass concentration (gray line: Qingyuan; light gray line: Guangzhou); (b) winds (vectors) and wind velocity (shadings; units: m s^{-1}); (c) temperature (shadings; units: °C); (d) RH (shadings; units: %); and (e) direct radiant exposure (of the vertical surface to the direction of solar radiation) and global radiant exposure. (Blue line: HPEs; white or red box: CSs; purple box: clearing; brown box: water vapor transport; and blue dot: precipitation)

Clearing pollution from Qingyuan depends on the lower strong northeasterly winds, which transport

dry, cold, and clean air to decrease temperature and RH and blow aerosol pollutants away from Qingyuan.

(Fig. 11 (b, d), purple boxes). In addition to the blowing effect of the cold northeasterly winds, the aerosol

pollution in Qingyuan is also affected by the mid-upper level sea flows, which enhance the atmospheric

RH to cause the PM$_{2.5}$ to enter the fog-cloud phase and possibly produce precipitation that eliminates

pollutants through wet removal (Fig. 11 (d), blue dots represent precipitation).

3.5   The two-way feedback is weakened by cloudy mid-upper layers in the humid Sichuan Basin. This area is capped by upper-level inversions caused air moving east across the Tibet Plateau.

Located in the upper reaches of the Yangtze River in southwestern China, the Sichuan Basin is a

lowland region surrounded by mountains on all sides (Fig. 2). Abutting the eastern edge of the Tibetan

Plateau to the west and northwest and the Daba Mountains and the Wu Mountains to the east and northeast, respectively (Fig. 2), the Sichuan Basin is rarely affected by cold northerly winds, which are blocked by the high mountains. On the southern and southeastern sides, the Sichuan Basin is flanked by the lower Yungui Plateau (Fig. 2), which is frequently affected by warm, humid southwesterly and southeasterly airflows from the Bay of Bengal and the southeastern sea. Transported water vapor from the south is blocked by the tall northern mountains and then accumulates in the Sichuan Basin. Located at the western edge of the Sichuan Basin, Chengdu is surrounded by the highlands to the south, the high and steep Longmen Mountains to the northwest, the Qionglai Mountains to the west, and the low Longquan Mountains to the east. The enclosed topographical features lead to a lower wind speed and a higher RH in Chengdu than in other parts of the Sichuan Basin.
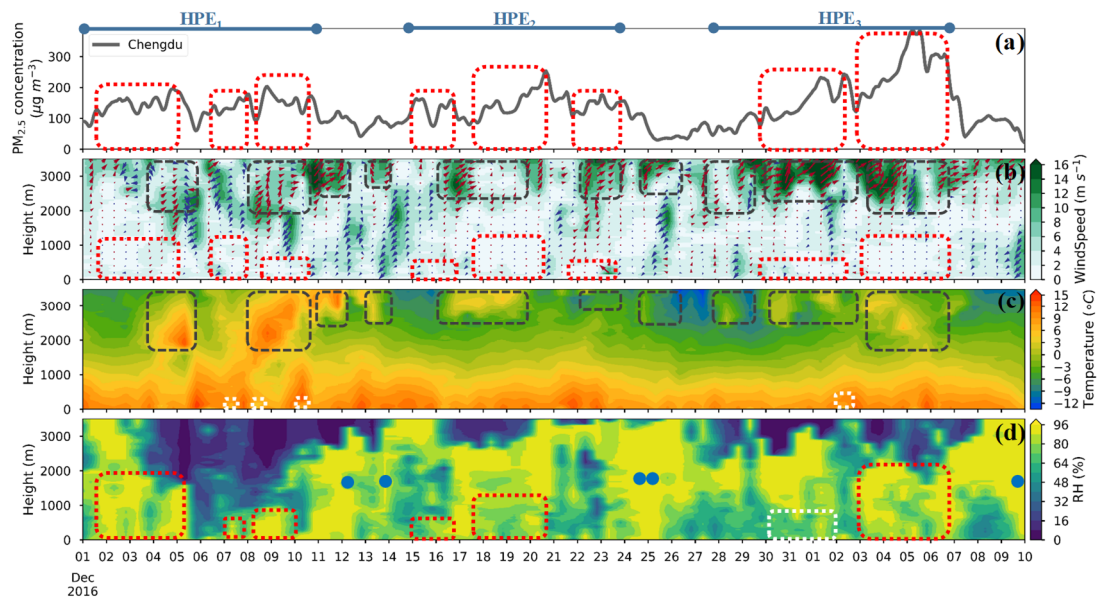
Figure 12: Temporal variations in PM2.5, surface radiation and vertical distributions of meteorological factors from December 1, 2016, to January 10, 2017. (a) PM2.5 mass concentration (gray line: Chengdu); (b) winds (vectors) and wind velocity (shadings; units: m s^{-1}); (c) temperature (shadings; units: ℃); (d) RH (shadings; units: %); and. (Blue line: HPEs; white or red box: CSs; brown box: warm air flow or inversions; and blue dot: precipitation.)

From December 1, 2016, to January 10, 2017, three HPEs appeared in Chengdu (Fig. 12, blue boxes), and these episodes lasted for more than 10 days and had peak mass concentrations greater than 200 μg m^{-3} (Fig. 12 (a)). During these three episodes, we observed thick mid-upper level fog/clouds above Chengdu (Fig. 12 (d)), which was blocked by the surrounding mountains and upper-level inversions. The mid-upper level cloud competes with the near-surface aerosols for solar radiation, i.e., as more solar radiation is reflected by the mid-upper layer cloud, the near-surface aerosols receive less solar radiation.

463   Therefore, with cloudy mid-upper layers, more solar radiation is reflected to cool the atmosphere below

464   the clouds, and this condition suppresses the two-way feedback mechanism between the unfavorable

465   weather conditions and the near-surface aerosols. Consequently, the two-way feedback was weak and

466   nearly no near-ground temperature inversion was observed (Fig. 12 (c)). Despite the lack of a two-way

467   feedback mechanism to aggravate aerosol pollution, the increase in the $PM_{2.5}$ mass concentration is still

468   under stable stratification dominated by slight or calm winds (Fig. 12, red boxes). Comparing the RH

469   variations in the two process of increasing $PM_{2.5}$ (Fig. 12 red boxes) during the HPE from December 26,

470   2016, to January 6, 2017, we found that the $PM_{2.5}$ mass concentration increases correspondingly with the

471   lower RH.
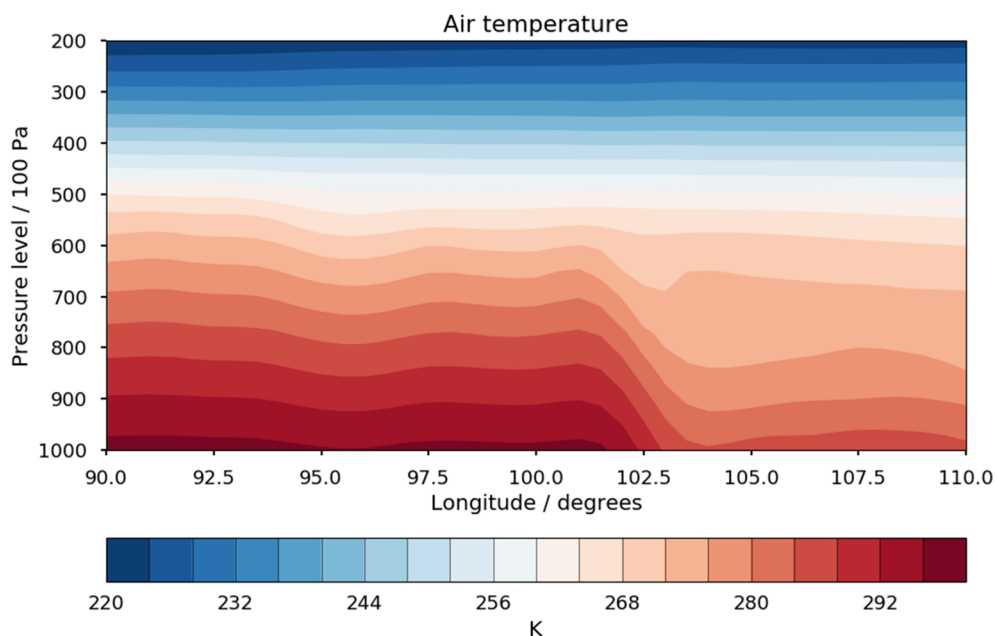
472

473   **Figure 13: Vertical section of mean air temperature in December 2016 at 30.67°N.**

474   In addition to the near-surface weak winds, persistent aerosol pollution is a result of temperature

475   inversions caused by the warm southwest advection (Fig. 12 (b, c), brown boxes). The ground of the

476   Qinghai-Tibet Plateau is a heat source throughout the year (Ye and Gao, 1979); thus, it heats the near-

477   surface ambient air (Fig. 13). When the relatively warm air moves east across the Tibet Plateau under the

478   southwesterly winds, it forms an inversion above the basin (Fig. 12 (c), brown boxes), which caps the

479   convective layer and then induces the accumulation of aerosols and water vapor.

480
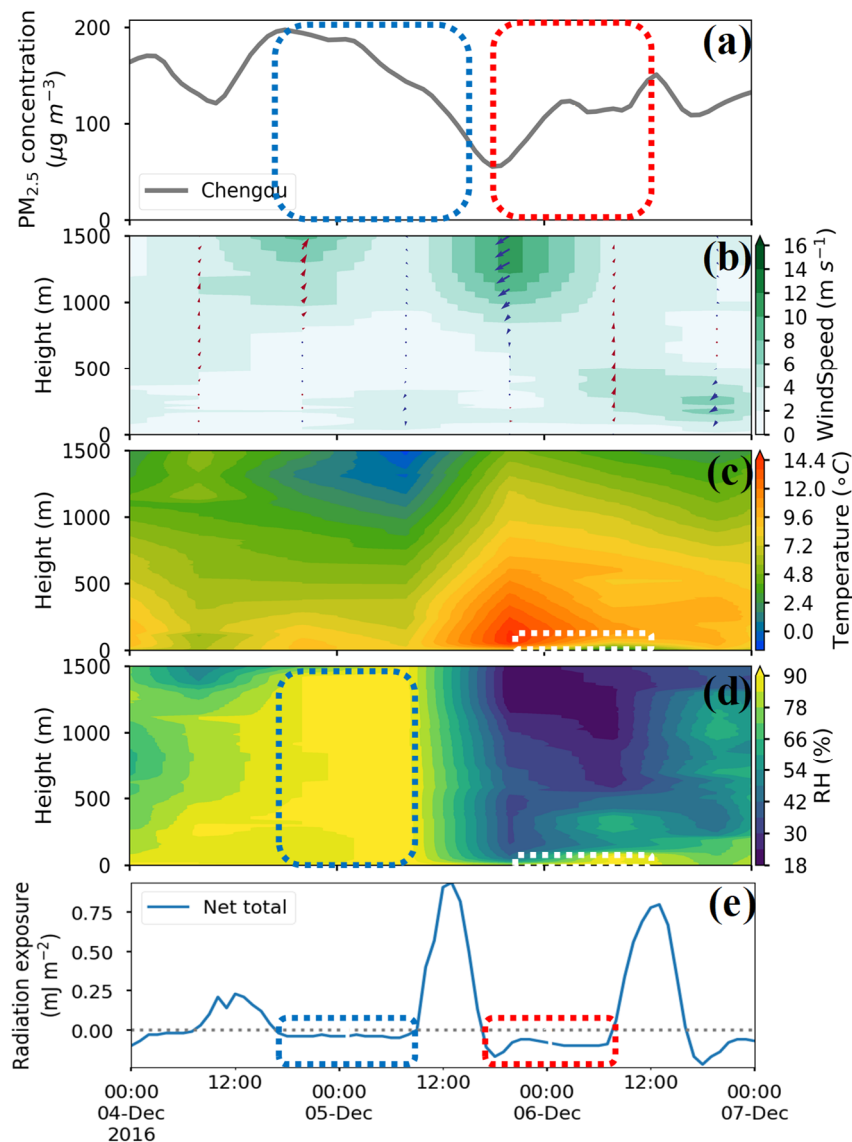
Figure 14: Temporal variations in PM₂.₅, surface radiation and vertical distributions of meteorological

factors from December 4 to 7, 2017. (a) PM₂.₅ mass concentration (gray line: Chengdu); (b) winds (vectors) and

wind velocity (shadings; units: m s⁻¹); (c) temperature (shadings; units: ℃); (d) RH (shadings; units: %); and (e)

global radiant exposure.

Effective pollution clearing rarely occurs in Chengdu because the Sichuan Basin is less affected by

the cold, clean northerly winds as a result of the surrounding high northern mountains. However, as soon

as aerosol pollutants and water vapor are cleared, aerosol pollution will form again due to more longwave

radiation lost from the ground. For example, during December 4-7, 2016, the fog/cloud dissipated, and

the PM₂.₅ mass concentration dropped to a low value on the 5th (Fig. 14 (a, d)). Due to the absence of

cloud/fog blocking, more longwave radiation from the ground was emitted into space on the 6th night,

and the surface net radiant exposure decreased from -0.58 on the 5th to -1.45 on the 6th (2.5 times) (Fig.

14 (e)). The significant reduction in the surface radiation cooled the near-surface atmospheric temperature, which formed an inversion layer of approximately 50~100 m (Fig. 14 (c)). Capped by the inversion layer, the PM$_{2.5}$ mass concentration doubled after the night of the 6th to form another aerosol pollution event ((Fig. 14 (a)).

Pollution removal in Chengdu mainly relies on northeasterly winds to blow pollution away. The winds also carry water vapor to add humidity to the atmosphere above Chengdu, which converts pollutants into fog/cloud drops or produces precipitation that removes pollutants through wet removal (Fig. 12 (d), blue boxes).

3.6 The two-way feedback mechanism on the windy Northeast China Plain, where mid-lower warm, humid southwesterly winds transport aerosol pollutants from polluted southwestern regions, and strong, clean northwesterly winds blow pollutants away.

The Northeast China Plain lies north of the Liaodong Gulf, west of the Changbai Mountains, east of the Greater Khingan, and south of the Lesser Khingan (Fig. 2). Due to the low mountains to the northwest, the Northeast China Plain is susceptible to cold, dry northerly air from Siberia in winter. As the largest city in Northeast China regarding its urban population, Shenyang is located in the southwestern Northeast China Plain (Fig. 2), where the warm, humid southwesterly flows are transported from Bohai Bay.
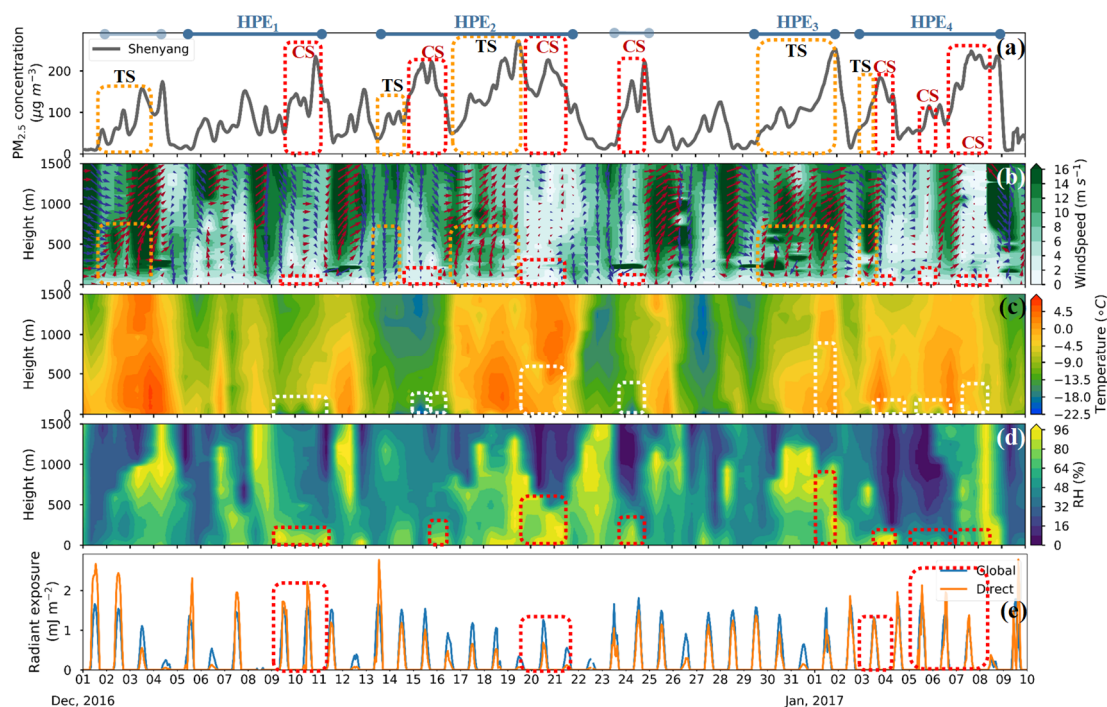
Figure 15: Temporal variations in PM$_{2.5}$, surface radiation and vertical distributions of meteorological factors from December 1, 2016, to January 10, 2017. (a) PM$_{2.5}$ mass concentration (gray line: Shenyang); (b)

winds (vectors) and wind velocity (shadings; units: m s^{-1}); (c) temperature (shadings; units: ℃); (d) RH (shadings; units: %); and (e) global radiant exposure. (Blue line: HPEs; light blue line: PEs; white or red box: CSs; and blue dot: precipitation)

From December 1, 2016, to January 10, 2017, six aerosol pollution episodes appeared in Shenyang (Fig. 15 (a), blue boxes), four of which persisted for more than 3 days with peak PM$_{2.5}$ mass concentrations greater than 200 μg m^{-3} (Fig. 15 (a)). During these HPEs, we observed surface radiation reductions, near-surface inversions, low-level RH enhancement, and increases in the PM$_{2.5}$ mass concentration (Fig. 15 (a, c, d), red and white boxes) under slight or calm winds (Fig. 15 (b), red boxes); these conditions indicate the occurrence of the two-way feedback mechanism in Shenyang.
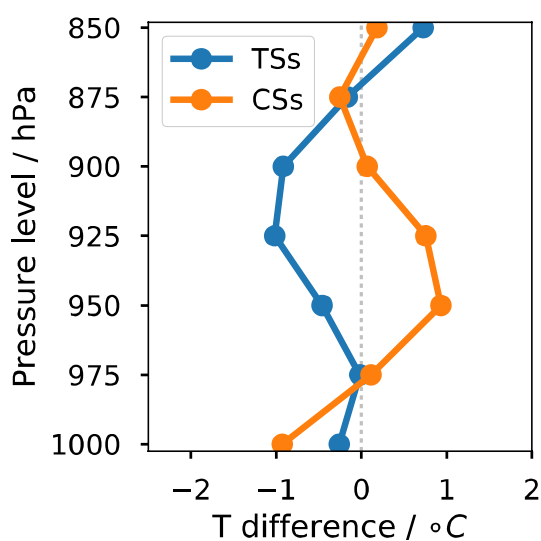
Figure 16: Vertical mean temperature difference between sounding observations and ERA-interim reanalysis data during TSs and CSs in Shenyang from December 1, 2016, to January 10, 2017.

To quantify the magnitude of the two-way feedback during TSs and CSs in Shenyang, the air temperature difference between the radiosonde observations at 2000 BJT and the ERA-interim reanalysis data was obtained. Similar to Beijing and Xi'an, the temperature profile was also modified by aerosols during both the TSs and the CSs (Fig.16 (a, b)). However, the magnitude of near-ground cooling bias was lower than that in Beijing and Xi'an, which is due to relatively light aerosol pollution and windy conditions. From TSs to CSs, the negative temperature difference at 1000 hPa increased from -0.26 ℃ to -0.93 ℃. The mean aerosol-induced cooling bias (1000 hPa) in the TSs was only 28.2% of that in the CSs.

Compared with those in Xi'an, Nanjing, Wuhan, Qingyuan, and Chengdu, the speeds of the southeasterly or northwesterly winds are strikingly higher in Shenyang. Relatively strong mid-lower southeasterly winds originate from Bohai Bay, and these winds transport warm, humid air that heats and

535   adds humidity to the mid-upper layer above Shenyang (Fig. 15 (c, d)). This air also transports aerosol

536   pollutants to Shenyang because it carries pollutants from populated and polluted southwestern industrial

537   regions, including Anshan. Lower strong northwesterly winds carry dry, cold air from Siberia to remove

538   pollutants in Shenyang (Fig. 15 (a, b)).

539   **3.7   Quantifying the two-way feedback mechanism and comparing its magnitude in various haze**
540   **regions of China.**

541   As previously mentioned, the weak two-way feedback mechanism in the Sichuan Basin is weakened

542   by the cloudy mid-upper layers, which compete with the near-surface aerosols for solar radiation.

543   However, the mechanism occurred in the Guanzhong Plain, the middle and lower reaches of the Yangtze

544   River, the Pearl River Delta region, and the Northeast China Plain. Dominant scattering aerosols will

545   scatter solar radiation to cause near-ground temperature reduction; Absorbing aerosols will absorb solar

546   radiation to heat the upper aerosol layer and subsequently cool the near-ground layer (Boucher et al.,

547   2013a). Previous studies found that aerosol profiles play an important part in radiative cooling effects of

548   aerosols, which results in vertical differences in meteorological factors (Wilcox et al., 2016;Wang et al.,

549   2018). To quantify the magnitude of the two-way feedback in these haze regions of China, we obtained

550   the vertical air temperature difference between the radiosonde observations affected by this two-way

551   feedback and the ERA-interim reanalysis data without feedback in the regional center cities, including

552   Beijing, Xi'an, Shenyang, Wuhan, Nanjing, and Qingyuan (to replace Guangzhou). A previous study

553   established a threshold value for the $PM_{2.5}$ mass concentration (100 μg m^{-3}) that effectively activates the

554   two-way feedback in HPEs; additionally, a lower threshold value (71 μg m^{-3}) has been identified for

555   lighter HPEs (Zhong et al., 2019). Therefore, based on the diurnal mean $PM_{2.5}$ mass concentration (from

556   08:00 to 17:00 BJT), the temperature difference is further classified by the criterion of 100 μg m^{-3} in the

557   more polluted North China Plain, Guanzhong Plain, and Northeast China Plain and by the criterion of 71

558   μg m^{-3} in the less polluted Two Lakes Plain, Yangtze River Delta, and Pearl River Delta.

559   By comparing the air temperature difference below and above these thresholds in the six cities, we

560   found that the lower temperature profile was strikingly modified by the two-way feedback mechanism

561   (Fig. 17). On the North China Plain, the Guanzhong Plain, and the Northeast China Plain, the lower

562   temperature bias between the sounding observations and the ERA-interim data was close to zero below

563   the threshold of 100 μg m^{-3} but immediately became negative above the threshold (Fig. 17 (a, b, c)). In

564 the Two Lakes Plain, the Yangtze River Delta, and the Pearl River Delta, we observed a similar reduction

565 in the temperature difference below and above the threshold of 71 μg m^{-3} (Fig. 17 (d, e, f)). Overall, the

566 magnitude of the two-way feedback mechanism was larger in the North China Plain, the Guanzhong

567 Plain, and the Northeast China Plain than in the Two Lakes Plain, the Yangtze River Delta, and the Pearl

568 River Delta.
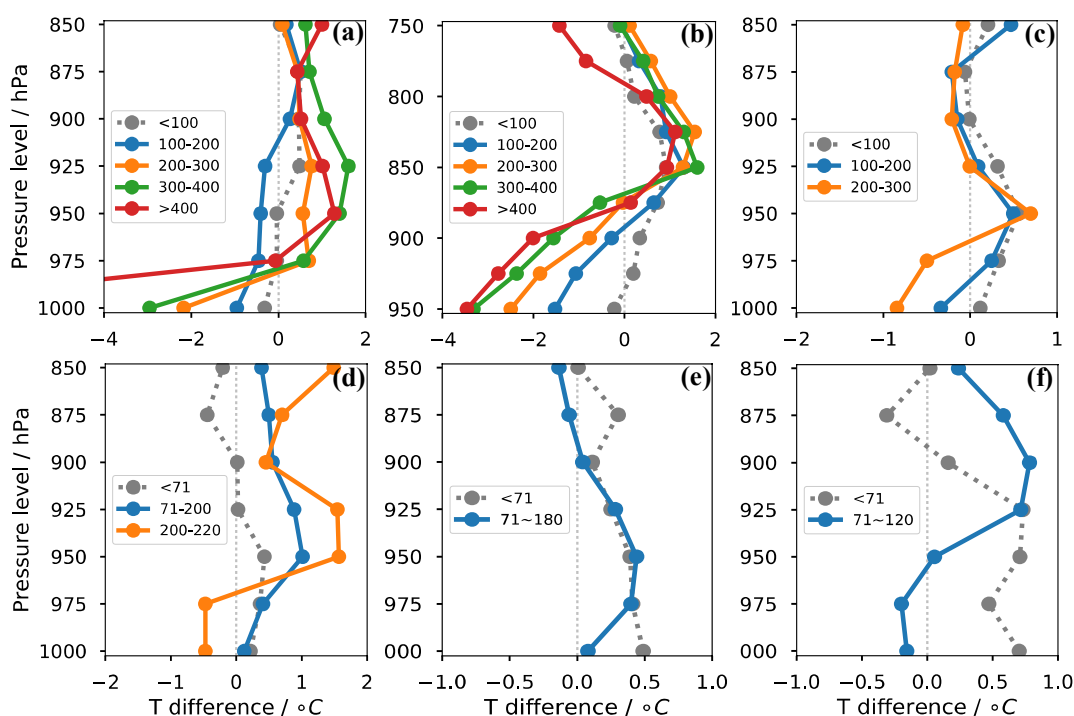
569

570 **Figure 17: Vertical temperature difference between sounding observations and ERA-interim reanalysis data**
571 **under different concentration bins of PM$_{2.5}$ mass (μg m^{-3}).** (a) Beijing; (b) Xi'an; (c) Shenyang; (d) Wuhan; (e)
572 Nanjing; and (f) Qingyuan.

573 For each representative site, the low-level cooling bias was more striking near the ground surface;

574 additionally, as the PM$_{2.5}$ mass concentration increased, the low-level cooling bias became more

575 significant (Fig. 17). In Beijing, the negative temperature difference reached more than 2℃ with PM$_{2.5}$

576 values in the range of 200 ~ 300 μg m^{-3} compared to approximately 1℃ in the range of 100 ~ 200 μg m

577 $^{-3}$. In Xi'an, the temperature difference decreased from approximately -1.5℃ in the range of 100 ~ 200

578 μg m^{-3} to 2.5℃ in the range of 200 ~ 300 μg m^{-3}. In Shenyang, the cooling bias of approximately 0.6℃

579 occurred with the increase in PM$_{2.5}$ from 100 ~ 200 μg m^{-3} to 200 ~ 300 μg m^{-3}. Under the most polluted

580 conditions, the near-ground cooling bias was greater than -4℃, approximately -4℃, and approximately

581 -1℃ in Beijing, Xi'an, and Shenyang, respectively, which was substantially affected by the two-way

582 feedback.

583   To quantify the feedback of the worsened meteorological conditions on the increasing $PM_{2.5}$ in the

584   CSs, a PLAM index was used, which mainly reflects the stability of the air mass and the condensation

585   rate of water vapor on aerosol particles. The squared correlation coefficients between the hourly PLAM

586   and $PM_{2.5}$ mass concentration in the typical $PM_{2.5}$ increase processes during the CSs were 0.71, 0.7, 0.72,

587   0.68, 0.64, and 0.63 in Beijing, Xi'an, Shenyang, Wuhan, Nanjing, and Qingyuan, respectively (Fig. 18

588   (a, b, c, d, e, f)); these values exceeded the 0.05 significance level, which suggested that such a

589   meteorological feedback on $PM_{2.5}$ explained 60~70% of the increase in the $PM_{2.5}$ during the CSs.
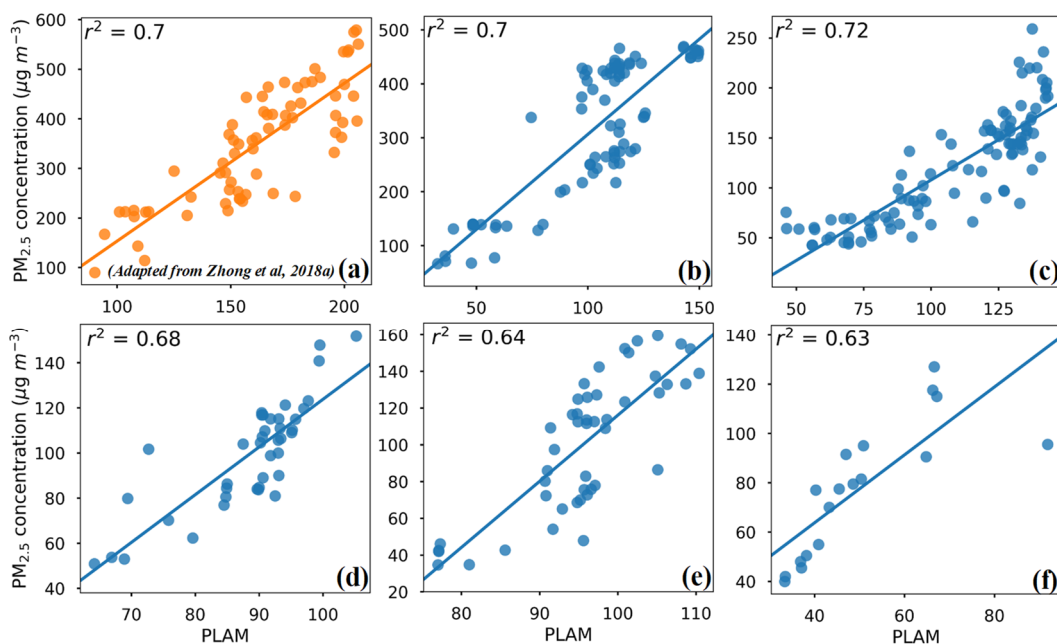
591   **Figure 18: Correlation between PLAM and $PM_{2.5}$ during the typical rising processes of $PM_{2.5}$ from**

592   **December 1, 2016 to January 10, 2017.**

593   **4 Conclusions:**

594   Here, we used $PM_{2.5}$ observations, surface radiation data, radiosonde observations, meteorological

595   index-PLAM, and ERA-interim reanalysis data to investigate the formation, accumulation, and

596   dispersion of aerosol pollution during persistent heavy aerosol pollution episodes over 3 days (HPEs),

597   particularly focusing on the two-way feedback mechanism between the unfavorable meteorological

598   conditions and the cumulative $PM_{2.5}$ pollution in various haze regions in China, including the Guanzhong

599   Plain, the Yangtze River Delta region, the Two Lakes Basin, the Pearl River Delta, the Sichuan Basin,

600   and the Northeast China Plain.

601   On the Guanzhong Plain, we observed a striking two-way feedback mechanism, including reduced

surface radiations, near-surface inversions, RH enhancement in the lower part of BL, and increases in $PM_{2.5}$ mass concentrations under slight or calm winds in the CSs. For the representative sites of Xi'an, the near-ground cooling bias caused by the two-way feedback was as high as approximately -4 ℃, which was similar to that observed in Beijing. Bordered by the Qinling Mountains and the Loess Plateau, the Guanzhong Plain experiences inter-regional pollution transport below the BL, e.g., pollution transport to Xi'an from Yuncheng and Linfen under lower northwesterly winds in the TSs. Pollution clearing mainly depends on the lower strong northeasterly winds to blow pollutants away and the mid-upper southerly winds to transport water vapor to increase RH, which causes the $PM_{2.5}$ to enter the fog-cloud phase.

In the relative less polluted Yangtze River Delta region, the aerosol pollution formation is similar to that in Beijing, including earlier TSs and later CSs. During the TSs, the Yangtze River Delta region is affected by trans-regional pollution transport below and over the BL from the North China Plain, which induces increases in the $PM_{2.5}$ in near-surface or at the higher atmosphere in this region, which includes Nanjing and Shanghai. Upper transported pollutants would move downward to worsen the near-ground aerosol pollution further. During the CSs, we also observed the two-way feedback mechanism, but its magnitude is lower than that in Beijing due to the less-polluted conditions. In this region, pollution clearing relies on persistent stronger northerly winds bring pollutants out of this area, or strong southeasterly winds, which transport clean, warm, humid air that blows pollutants away or increases ambient RH to cause the $PM_{2.5}$ to enter the liquid fog-cloud phase. Similar to the Yangtze River Delta region, the Two Lakes Basin also experienced trans-regional pollution transport from the North China Plain under northerly winds below and sometimes over the BL during the TSs. During the CSs, the two-way feedback is activated, and the aerosol pollution worsens. In addition to the blowing effect of strong, persistent northerly winds, pollution clearing also depends on the mid-upper southerly winds, particularly the southwesterly winds, to transport water vapor, which enhances the RH and eliminates pollutants through fog-cloud conversion and wet removal.

In the least polluted Pearl River Delta, no feedback mechanism was observed with $PM_{2.5}$ mass concentrations below the threshold. However, when the $PM_{2.5}$ concentration exceeded the threshold, the two-way feedback occurred in the CSs. The delta region was purified by lower clean, cold northeasterly winds from the northern mountains and humidified by upper southerly winds from the South China Sea.

The Sichuan Basin is dominated by high RH and weak winds; thus, the two-way feedback

631 mechanism was weakened by thick mid-upper fog/clouds that compete with the near-surface aerosols for

632 solar radiation and consequently cool the whole atmosphere below. With the weak two-way feedback,

633 the PM$_{2.5}$ mass concentration increased under lower slight or calm winds and was capped by the upper

634 temperature inversions caused by the upper southwesterly winds from the Tibet Plateau. Pollution

635 clearing mainly relies on northeasterly winds to blow pollutants away, and these winds also add humid

636 air to the atmosphere, which converts aerosols into fog/cloud drops. Although pollutants and water vapor

637 are cleared, aerosol pollution will soon form again due to more longwave radiation lost from the ground,

638 which results in rare effective pollution clearing in the Sichuan Basin.

639   Compared with the above regions, the southerly and northerly winds are strikingly larger in the

640 Northeast China Plain. Strong mid-lower southeasterly winds originate from Bohai Bay, transport warm,

641 humid air that heats and adds humidity to the inland area and transport pollutants inter-regionally from

642 polluted southwestern industrial regions. Lower strong northwesterly winds carry dry, cold air from

643 Siberia to remove pollutants. At the representative site in Shenyang, a two-way feedback mechanism also

644 exists during the CSs with slight or calm winds.
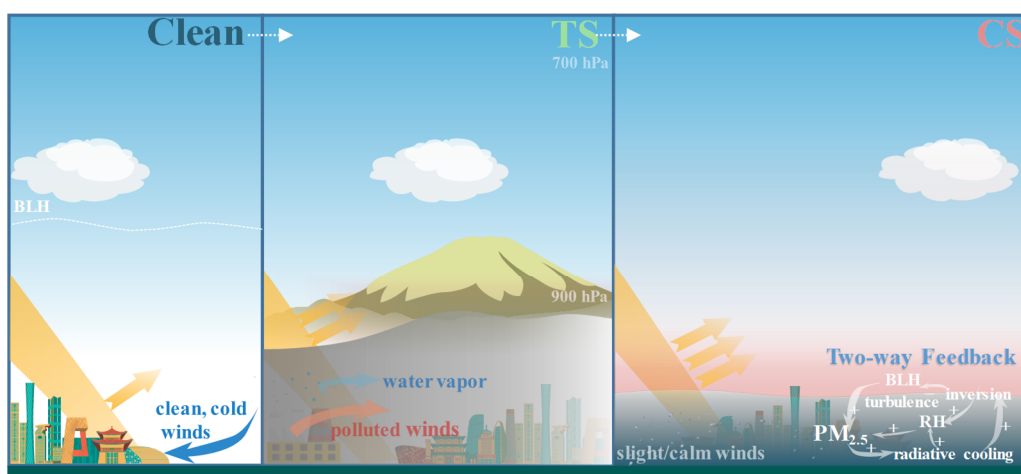
645

646 **Figure 19: A concept scheme of pollution removal (a), transport (b), and accumulation (c), particularly the**

647 **two-way feedback mechanism between the unfavorable meteorological conditions and the cumulative**

648 **aerosol pollution (c).**

649   The transport, accumulation, and removal of pollution described above are visually illustrated in a

650 conceptual scheme (Fig. 19), which particularly highlights the effect of the two-way feedback mechanism

651 in the role of intensifying the HPEs. Due to the occurrence of a two-way feedback mechanism, effective

652 pollution control could further mitigate aerosol pollution, while persistent worsening aerosol pollution

653   could lead to an additional increase in $PM_{2.5}$. Given the inter-regional and trans-regional pollution

654   transport, the control of regional emissions among key haze regions in China, to reduce the pollutants

655   transport or to let them not reach the threshold enough to trigger two-way feedback mechanism, is

656   essential to reduce persistent heavy aerosol pollution episodes substantially. At the same time, these

657   results also show that, even in favorable weather conditions, aerosol pollutant emissions should not be

658   allowed to occur without restrictions; when aerosol pollution cumulates to a certain extent, it will

659   significantly worsen the BL meteorological conditions and "close" the "meteorological channels"

660   available for pollution dispersion.

661

662   **Acknowledgment:**

663   This research is supported by the National Key Project of MOST (2016YFC0203306) and the

664   Atmospheric Pollution Control of the Prime Minister Fund (DQGG0104).

665   **Author Contributions:**

666   X.Y.Z. and Y.Q.W. designed the research; X.Y.Z and J.T.Z carried out the analysis of observations.

667   T.J.W provided UAV observations. J.Z.W provided PLAM data. X.J.S conducted a supplementary

668   analysis. J.T.Z. wrote the first manuscript and X.Y.Z. revised it. All authors contributed to the

669   improvement of this manuscript and approved the final version.

670   **Additional Information:**

671   Competing financial interests: The authors declare no competing financial interests.

672

References:

Bai, N., et al.: The pharmacology of particulate matter air pollution-induced cardiovascular dysfunction, Pharmacol. Ther., 113, 16-29, 2007.

Boucher, O., et al.: Clouds and aerosols, in: Climate change 2013: the physical science basis. Contribution of Working Group I to the Fifth Assessment Report of the Intergovernmental Panel on Climate Change, Cambridge University Press, 571-657, 2013a.

Boucher, O., et al.: Clouds and Aerosols, in: Climate Change 2013: The Physical Science Basis. Contribution of Working Group I to the Fifth Assessment Report of the Intergovernmental Panel on Climate Change, edited by: Stocker, T. F., Qin, D., Plattner, G.-K., Tignor, M., Allen, S. K., Boschung, J., Nauels, A., Xia, Y., Bex, V., and Midgley, P. M., Cambridge University Press, Cambridge, United Kingdom and New York, NY, USA, 571–658, 2013b.

Chen, Y., et al.: Evidence on the impact of sustained exposure to air pollution on life expectancy from China's Huai River policy, PNAS, 110, 12936-12941, 10.1073/pnas.1300018110, 2013.

Cheng, Y., et al.: Reactive nitrogen chemistry in aerosol water as a source of sulfate during haze events in China, Sci. Adv., 2, e1601530, 10.1126/sciadv.1601530, 2016.

Dee, D. P., et al.: The ERA-Interim reanalysis: configuration and performance of the data assimilation system, Q. J. R. Meteorolog. Soc., 137, 553-597, doi:10.1002/qj.828, 2011.

Ding, A. J., et al.: Enhanced haze pollution by black carbon in megacities in China, Geophys. Res. Lett., 43, 2016.

Ervens, B., et al.: Secondary organic aerosol formation in cloud droplets and aqueous particles (aqSOA): a review of laboratory, field and model studies, Atmos. Chem. Phys., 11, 11069-11102, 10.5194/acp-11-11069-2011, 2011.

Fang, S., et al.: Parameterization and comparative evaluation of the CCN number concentration on Mt. Huang, China, Atmos. Res., 181, 300-311, 10.1016/j.atmosres.2016.07.004, 2016.

Huang, X., et al.: Impact of Aerosol-PBL Interaction on Haze Pollution: Multiyear Observational Evidences in North China, Geophys. Res. Lett., 0, doi:10.1029/2018GL079239, 2018.

Ji, D., et al.: The heaviest particulate air-pollution episodes occurred in northern China in January, 2013: insights gained from observation, Atmos. Environ., 92, 546-556, 2014.

Kuang, Y., et al.: Impact of aerosol hygroscopic growth on the direct aerosol radiative effect in summer on North China Plain, Atmospheric Environment, 147, 224-233, 2016.

Matus, K., et al.: Health damages from air pollution in China, Global Environ. Change, 22, 55-66, 2012.

Pilinis, C., et al.: Water content of atmospheric aerosols, Atmos. Environ., 23, 1601-1606, 1989.

Poli, P., et al.: Assimilation of Global Positioning System radio occultation data in the ECMWF ERA–Interim reanalysis, Q. J. R. Meteorolog. Soc., 136, 1972-1990, 2010.

Simmons, A.: ERA-Interim: New ECMWF reanalysis products from 1989 onwards, ECMWF newsletter, 110, 25-36, 2006.

Su, F., et al.: Transport pathways of pollutants from outside in atmosphere boundary layer, Res. Environ. Sci., 1, 26-29, 2004.

Tao, S.: Error Analyses for Temperature of L Band Radiosonde, Meteorological, 2006.

Thépaut, J. N., et al.: Dynamical structure functions in a four-dimensional variational assimilation: A case study, Q. J. R. Meteorolog. Soc., 122, 535-561, 1996.

Tie, X., et al.: Severe Pollution in China Amplified by Atmospheric Moisture, Sci. Rep., 7, 15760, 10.1038/s41598-017-15909-1, 2017.

717 Wang, J., et al.: Diagnostic identification of the impact of meteorological conditions on PM2.5
718 concentrations in Beijing, Atmos. Environ., 81, 158-165, 10.1016/j.atmosenv.2013.08.033, 2013.
719 Wang, J. Z., et al.: A parameterized method for air-quality diagnosis and its applications, Advance
720 of Meteorology, doi:10.1155/2012/238589, 1-10, 2012.
721 Wang, Z., et al.: Dome effect of black carbon and its key influencing factors: a one-dimensional
722 modelling study, Atmos. Chem. Phys., 18, 2821-2834, 10.5194/acp-18-2821-2018, 2018.
723 Wilcox, E. M., et al.: Black carbon solar absorption suppresses turbulence in the atmospheric
724 boundary layer, Proceedings of the National Academy of Sciences, 113, 11794-11799, 2016.
725 Yang, Q., et al.: Spatial distribution pattern of population and characteristics of its evolution in
726 China during 1935-2010, Geographical Research, 35, 1547-1560, 2016.
727 Ye, D., and Gao, Y.: Meteorology of the Tibetan Plateau, Science Publication Agency, Beijing (in
728 Chinese). Google Scholar, 1979.
729 Zhang, Q., et al.: Asian emissions in 2006 for the NASA INTEX-B mission, Atmos. Chem. Phys., 9,
730 5131-5153, 2009a.
731 Zhang, Q., et al.: Cleaning China's air, Nature, 484, 161, 10.1038/484161a, 2012a.
732 Zhang, X., et al.: Factors contributing to haze and fog in China, Chin. Sci. Bull., 58, 1178,
733 10.1360/972013-150, 2013.
734 Zhang, X. Y., et al.: Changes of Atmospheric Composition and Optical Properties Over BEIJING—
735 2008 Olympic Monitoring Campaign, Bull. Am. Meteorol. Soc., 90, 1633–1651, 2009b.
736 Zhang, X. Y., et al.: Atmospheric aerosol compositions in China: spatial/temporal variability,
737 chemical signature, regional haze distribution and comparisons with global aerosols, Atmos. Chem.
738 Phys., 12, 779-799, 10.5194/acp-12-779-2012, 2012b.
739 Zhang, X. Y., et al.: Changes in chemical components of aerosol particles in different haze regions
740 in China from 2006 to 2013 and contribution of meteorological factors, Atmos. Chem. Phys., 15,
741 12935-12952, 10.5194/acp-15-12935-2015, 2015.
742 Zhong, J., et al.: Relative contributions of boundary-layer meteorological factors to the explosive
743 growth of PM 2.5 during the red-alert heavy pollution episodes in Beijing in December 2016, J.
744 Meteorolog. Res., 31, 809-819, 2017.
745 Zhong, J., et al.: Feedback effects of boundary-layer meteorological factors on cumulative
746 explosive growth of PM2.5 during winter heavy pollution episodes in Beijing from 2013 to 2016,
747 Atmos. Chem. Phys., 18, 247-258, 10.5194/acp-18-247-2018, 2018a.
748 Zhong, J., et al.: Heavy aerosol pollution episodes in winter Beijing enhanced by radiative cooling
749 effects of aerosols, Atmos. Res., 209, 59-64, https://doi.org/10.1016/j.atmosres.2018.03.011,
750 2018b.
751 Zhong, J., et al.: Reflections on the threshold for PM2.5 explosive growth in the cumulative stage
752 of winter heavy aerosol pollution episodes (HPEs) in Beijing, Tellus B: Chemical and Physical
753 Meteorology, 71, 1-7, 10.1080/16000889.2018.1528134, 2019.
754 Zhou, S., et al.: The Characteristics and Contributing Factors of Air Pollution in Nanjing: A Case
755 Study Based on an Unmanned Aerial Vehicle Experiment and Multiple Datasets, Atmosphere, 9,
756 343, 10.3390/atmos9090343, 2018.
757 Zhu, W., et al.: The characteristics of abnormal wintertime pollution events in the Jing-Jin-Ji region
758 and its relationships with meteorological factors, Sci. Total Environ., 626, 887, 2018.
759